MODELING AND EXPERIMENTING A NOVEL INVERTED DRIFT TUBE DEVICE FOR IMPROVED MOBILITY ANALYSIS OF AEROSOL PARTICLES

A Thesis

Submitted to the Faculty

of

Purdue University

by

Md Minal Nahin

In Partial Fulfillment of the

Requirements for the Degree

of

Master of Science in Mechanical Engineering

December 2017

Purdue University

Indianapolis, Indiana

THE PURDUE UNIVERSITY GRADUATE SCHOOL
STATEMENT OF COMMITTEE APPROVAL

Dr. Carlos Larriba-Andaluz, Chair

Department of Mechanical Engineering

Dr. Hazim El-Mounayri

Department of Mechanical Engineering

Dr. Whitney Yu

Department of Mechanical Engineering

Approved by:

Dr. Sohel Anwar

Chair of the Graduate Program

To my beloved parents, brother and sister

ACKNOWLEDGMENTS

First, I would like to thank Almighty for giving me the strength, ability and opportunity to undertake this research study, to hold on and finish it. I would like to express my sincere gratitude to my thesis advisor, Dr. Carlos Larriba-Andaluz, for his proper guidance, cooperation, and support towards the completion of this thesis work. In every step of my research work, I found him as a person of immense knowledge and critical problem-solving abilities. I would like to thank him for keeping faith upon me until the end of this work. I would also like to thank my lab-mates Joseph Derrick, Vaibhav Shrivastav, Xi Chen, and Tianyang Wu for their precious time and support towards my research work. I got immense help from Joseph and Vaibhav with my experiment set-up and execution. They were always ready to help and kept me motivated towards my goal both by serious and amusing means. Tianyang Wu and Xi Chen also helped me a lot during experiments. I am grateful to my parents for their endless support and for being a source of inspiration for me to pursue my dream and hard work. Without their continuous encouragement, this accomplishment would never come true.

TABLE OF CONTENTS

Page

LIST OF TABLES

LIST OF FIGURES

Figure Page

SYMBOLS

m_{red}	reduced mass of ion
v_{drift}	ion drift velocity
v_{gas}	drift gas velocity
K_0	ion mobility at standard temperature and pressure
K	reduced ion mobility
L	drift tube length
E	electric field
P	pressure
T	temperature
t	time
q	ion charge
e	electron charge
ρ_{gas}	gas density
Ω	collision cross section
μ	dynamic viscosity
d_p	ion diameter
d_{ion}	ion diameter
d_{gas}	gas diameter
λ	mean free path
n	distribution of ions
D_L	longitudinal diffusion coefficient
A	electric field slope
$\bar{x}$	mean position of ions
Σ	standard deviation
R	resolution

Λ	separation ratio
v_m	relative velocity of ion
$\bar{v_{ion}}$	ion average thermal speed
k	Boltzmann constant
ν_{rate}	collision frequency
N	number density of gas
b_o	time constant
R_P	resolving power
x_p	distanced travelled by ion
t_{end}	time needed to reach the detector
t_{delay}	delay time
n_p	number of electrode

ABBREVIATIONS

IMS	Ion Mobility Spectrometry
MS	Mass Spectrometry
IMMS	Ion Mobility Mass Spectrometry
ESI	Electro-spray Ionization
DTIMS	Drift Tube Ion Mobility Spectrometry
TIMS	Trapped Ion Mobility Spectrometry
FAIMS	Field Asymmetric Waveform Ion Mobility Spectrometer
OLIMS	Open Loop Ion Mobility Spectrometry
DMA	Differential Mobility Analyzer
IDT	Inverted Drift Tube
IPS	Intermittent Push Flow Separation
NSP	Nearly Stopping Potential
FWHM	Full Width at Half Maximum
RF	Radio Frequency
SDS	Statistical Diffusion Simulation
CFD	Computational Fluid Dynamics
1D	One Dimensional
2D	Two Dimensional
3D	Three Dimensional
ADC	Analog to Digital Converted
DAQ	Data Acquisition

ABSTRACT

Nahin, Md Minal. M.S.M.E., Purdue University, December 2017. Modeling and Experimenting a Novel Inverted Drift Tube Device for Improved Mobility Analysis of Aerosol Particles. Major Professor: Carlos Larriba-Andaluz.

Ion Mobility Spectrometry (IMS) is an analytical technique for separation of charged particles in the gas phase. The history of IMS is not very old, and in this century, the IMS technique has grown rapidly in the advent of modern instruments. Among currently available ion mobility spectrometers, the DTIMS, FAIMS, TWIMS, DMA are notable. Though all the IMS systems have some uniqueness in case of particle separation and detection, however, all instruments have common shortcomings. They lack in resolution, which is independent of mobility of different charged particles and they are not able to separate bigger particles (20 120 nm) with good accuracy. The work presented here demonstrates a new concept of IMS technique at atmospheric pressure which has a resolution much higher than that of the currently available DTIMS (Drift Tube Ion Mobility Spectrometry) instruments. The unique feature of this instrument is the diffusion auto-correction. Being tunable, It can separate the wide range of particles of different diameters. The working principle of this new IMS technique is different from the typical DTIMS and to simply put, it can be considered as an inversion of commonly used technique, so termed as Inverted Drift Tube (IDT).The whole work performed here can be divided into three major phases. In the first phase, the analytical solution was derived for two new separation techniques: IPF (Intermittent push flow) and NSP (Nearly stopping potential) separations. In the next phase, simulations were done to show the accuracy of the analytical solution. An ion optics simulator software called SIMION 8.1 was used for conducting the simulation works. These simulations adopted the statistical diffusion

(SDS) collision algorithm to emulate the real scenario in gas phase more precisely. In the last phase, a prototype of experimental setup was built. The experimental results were then validated by simulated results.

1. INTRODUCTION

1.1 Historical Background of Ion Mobility Spectrometry

Ion mobility spectrometry (IMS) is a widely used analytical technique to separate and classify ionized particles in the gas phase based on their size and shape. Separation of charged nanoparticles occurs at atmospheric pressure when the charged particles drift through a buffer gas under the influence of an electrical field [1–5]. Previously, this separation technique was called plasma chromatography. The first trace of IMS was found in 1889 when Rutherford tried to investigate the ionization of gases and the conduction of electricity through that [6]. Later, these ionization work continued by Rutherford himself, Zeleny, frank, Tyndall, Townsend, and Thomson through different methodologies [7]. As an aftermath of several trials, the IMS measurements got its shape both theoretically and experimentally. In 1970s Karasek invented a new technique to use IMS as a qualitative detector for liquid and gas chromatography. He also continued his work to combine IMS (Ion mobility spectrometry) with MS (Mass spectrometry) and created IMMS system. In 1980, ESI (electrospray ionization) unfolded a new horizon for ionization of complex nonvolatile system. Shummate in 1989 coupled ESI with IMS. Wu and Chen later paired ESI with IMMS (Ion Mobility Mass Spectrometry) system, where, they were able to detect the mass-identified mobility peaks with fair resolving power [8,9]. The rapid advances in IMS occurred in the 20th century. A wide variety of instruments and instrumentation techniques were developed very rapidly. Among them, the most notable are Traveling-Wave IMS [10, 11], High Field Asymmetric waveform Ion Mobility Spectrometer (FAIMS) [12], Trapped Ion Mobility Spectrometer (TIMS) [13], Open Loop IMS (OLIMS), and Differential Mobility Analyzer (DMA) [14].

IMS has its greatest impact in the sector of security [15, 16]. It is the best choice for detecting narcotics, explosives, chemical, and biological warfare agents [6]. IMS is widely used in airports as well as customs. The interesting part of IMS is that it can detect any substances, which can be ionized. It can be used for analysis of lightest element like Helium to most complex mixtures, for example, proteomes, metabolomes.

In biology, IMS is used to determine cell, fungi, bacteria by the enzyme-substrate reaction. In medicine, it is widely used for detecting drugs in the breath of patients and volatile metabolites to diagnose different diseases. In food and beverage industries, it is also used for detecting different chemicals such as acetaminophen, aspartame, caffeine, glucosamine, etc. IMS can also detect the airborne molecular contamination as well as inorganic species such as Chlorine, Bromine, Hydrogen Fluoride, Nitrogen dioxide, Florine, Chlorine, iodine, Hydrogen bromide, etc [6]. Due to easy, low-cost operation and quick detection, these IMS techniques have become a promising tool for conducting research. Currently, IMS is not only being used for separating and detecting the charged nano-particles rather, it is also being used for calculating the collision cross section of molecules which is very important to predict the collision behavior as well as transport properties of molecules [11].

1.1.1 Theoretical Consideration of a Drift Tube Ion Mobility Spectrometer

The most basic instrument for IMS technique is drift-tube ion mobility spectrometer. In a typical Drift tube ion mobility spectrometer (DTIMS), Ions get push by constant electric field and drift through a buffer gas at atmospheric pressure. In a drift tube instrument, different ions take different time to travel through the buffer gas based on their shapes and sizes. The bigger ions face the huge number of collision with the buffer gas particles and thereby lag behind. On the other hand, smaller ions move ahead due to less number of collision with the buffer gas particles and take less time to reach the detector. These characteristics can better be explained by a simple

term mobility. Mobility can be defined as the terminal velocity of an ion when it is pushed by a constant electric field and drifts through a buffer gas. By equation we can represent the mobility as:

$$v_{drift} = K_0 E \tag{1.1}$$

Where the v_{drift} is the velocity of gas. K_0 represents the mobility of particles at standard temperature 273.15K and standard pressure 760mm(Hg) and E represents electric field. It is quite evident from the formula that, if the electric field is constant then the v_{drift} is directly proportional to Mobility term K meaning, higher the mobility the greater the drift velocity Now if the drift length is L and drift time for any particular ion is t then it can be written,

$$v_{drift} = L/t \tag{1.2}$$

If the applied voltage across the drift cell is V then the electric field can also be written as,

$$E = V/L \tag{1.3}$$

Combing equation 1.2 and 1.3,

$$K_0 = L^2/Vt \tag{1.4}$$

For any local temperature T and local pressure P the reduced mobility K can be calculated as follow:

$$K = K_0(P/760)(273.15/T) \tag{1.5}$$

From equation 1.4 if the voltage V and Length L are kept constant then the mobility would only be a function of time t. Therefore, If a particle would take more time t to cover length L then, the particle would have lower mobility and vice versa. Using this concept experimentally the mobility can be calculated.

Theoretically, the mobility of any ion or particle depends on many other factors and the relation is not that straightforward like the experimental mobility calculation. The slower or faster movement of any ion or particle is dependent on size, shape,

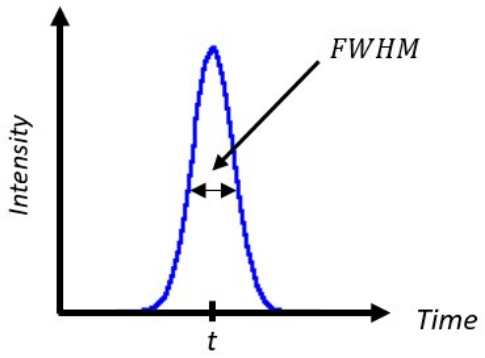

Figure 1.1. Peak distribution and resolution

mass, charge, etc. of that ion. Theoretically, in free molecular regime according to Mason-Scamp the mobility can be defined also as,

$$K = 3qe/(4\rho_{gas}\Omega)\sqrt{\pi m_{red}/8kT} \tag{1.6}$$

Where K is mobility, m_{red} is the reduced mass of ion in drift gas, k is Boltzmann constant, T is buffer gas temperature in kelvin, q is the charge of ion, ρ_{gas} is the mass density, and Ω is collision cross section (CCS) of the ion. The experimentally found Mobility value is used to find the collision cross-section of a particular ion or particle. One very important parameter to determine the capability of an IMS instrument is the resolution. The resolution is calculated for an IMS instrument to find its relative ability of separate and detect different ions. The resolution of typical drift tube spectrometer can be defined as [17],

$$R = t/FWHM \tag{1.7}$$

Here, $FWHM$ is the full width of the IMS peak at half maximum and t is the average time counted for the peak distribution. Figure 1.1 shows the peak distribution, peak width at half maximum ($FWHM$) and average time t. The resolution of IMS instrument can vary from 40 to 150. IMS can also be coupled with MS for more better resolution.

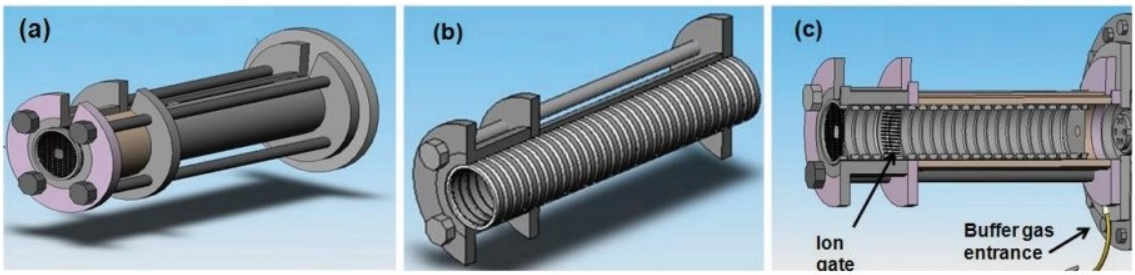

Figure 1.2. a) Drift Tube of an Ion Mobility Spectrometer. b) Guard Rings inside the Drift Tube. c) Section View [6].

1.2 Different Common Parts of IMS Instrument

Any IMS instrument has some parts in common. They are ionization source, drift cell, ion gate and ion detector.

Ionization Source

ESI or electro-spray is the common source of ionization widely used for Mass spectrometry instrument. In ESI, the high voltage is applied into a solution or liquid to create charged aerosol particles under the influence of pressure [18]. By tuning the voltage and pressure, a stable Taylor Cone [19] can be found which is mandatory for getting good signals. Figure 1.3 shows the electrospray ionization process. Nickel-63 is another common ionization source which is a radioactive source which emits beta ray [6]. The collision of the particle with the electron from beta ray convert the particles into the positive ion. These ions are then separated in drift cell. One advantage of Ni63 source is it requires no external power supply like the ESI. However, extra caution is necessary for the radioactive source.

Another common ionization source is corona discharge ionization. Like ESI a high voltage is applied to a needle produces a corona around the needle tip owing to the high electric field. It generally produces high electric field.

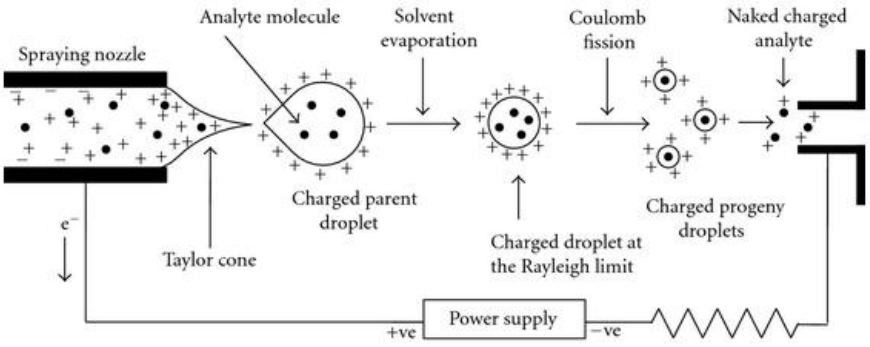

Figure 1.3. Electrospray ionization process [20].

Drift Cell

The drift consists of several ring electrodes. Figure 1.2 (b) and (c) show the drift cell with ring electrodes. To avoid voltage leaking one spacer is placed between two electrodes. Voltage is applied to the ring electrodes and the distribution of voltages over the electrodes are ensured by resistors. In DTIMS, the voltage linearly decreases towards the downstream side to keep the electric field constant inside. In a typical IMS instrument, the voltage applied to the ring electrodes creates an electric field that pushes ions to drift through the buffer gas. The voltages in the ring electrodes can be tuned based on the size of ions to be separated or detected. Typically, high voltage in the ring electrodes is applied for detecting the low mobility or bigger sized particles. Small voltage or electric field is needed to capture high mobility particles that are much smaller.

Ion Gate

Ion gate is used to on and off the flow of ions inside the drift cell. The most commonly used IMS ion gate is Barbury-Nielsen (BN) gate. In BN gate, a series of parallel wires are arranged in the perpendicular direction of ion flow. In any two consecutive wires, one contains positive, and another contains negative voltage. Due to this positive and negative voltage ions get deflected from their way and cannot pass through the detector which is the gate close stage. When no voltage is applied to the wires then it is open for the ions to go through which is the open stage. Typically, $\pm$ 25 to 100V is applied in BN gate wires [6].

Pulsing is another popular gating system for the IMS system. A high voltage pulse restricts the ions to go into the drift cell and when no voltage is applied the ions can pass through. In both BN and pulse gate system, the voltage applied is proportional to the size of particles. Higher voltage is applied in BN gate for shutting down the flow of ions.

Ion Detector

The most common detector for ion in IMS system is Faraday plate combined with an aperture grid. Altogether, it is called Faraday cage which is common in DTIMS, FAIMS instruments. In Faraday cage, ions are allowed to impact a metal plate which is grounded in a current to voltage amplifier. The charge imparted on the plate by the impact is amplified, and the resulting signal is plotted versus time to produce an IMS spectra. One disadvantage of Faraday cage is, it can only detect positive ions. For detecting both positive and negative ions at the same time, electro-meter pico-ammeters can also be used [6]. In addition, one mass spectrometer system can be used at the end of IMS instrument to detect the ions. After detection and amplification, the signal turns into a peak in a recorder. The area of the peak represents the concentration of the identified compound and the position of the peak represents the compound size, and shape as the arrival time to the detector is proportional to the mobility for any ion.

1.3 Drawbacks of Typical IMS System and The Characteristics New IMS Instrument

Mobility is the key factor for determining the particle size distribution in any IMS instrument. Considering the globular shape of a particle a particles electrical mobility can be linked to its diameter, d_p through the well-known equation in Aerosol science [14, 21].

$$K = qeC_C(K_n, \lambda, d_p)/(3\pi\mu d_p) \tag{1.8}$$

Where, K is mobility, qe is the net charge on the particle (product of the integer charge state and the unit electron charge), μ is the dynamic viscosity and λ is the mean free path. C_c represents Cunninghams correction factor and is a function of the Knudsen number.

Most often, mobility based size distribution functions are measured with differential mobility analyzers (DMA) [22] coupled to Condensation Nucleus Counters

CNCs [23]. DMA can also be operated in series as a scanning mobility particle sizer (SMPS) [24]. SMPS combination technique has become very successful for separating and detecting particles, however, there are several shortcomings to its use which could be improved upon employing different techniques. It is because the in DMA the sheath velocity and distance to cover by a particle are both constant that ultimately make the resident time inside the DMA constant for all types of particle. As a result, the diffusion broadening becomes huge which obviously degrades the resolution especially for sub 20nm particles [25, 26].

In most commercial devices for detecting the particles larger than 20nm, the resolution, defined as fixed $K/\Delta K$ is approximately less than 10. This results in the adequate resolution but sometimes insufficient -a 90nm mono-disperse distribution is not distinguishable from a 100nm mono-disperse distribution.

Scanning time is another issue for IMS instruments. Even in faster scanning instruments, particles of different sizes are sampled at different times, for example, a regular Drift tube spectrometer suffers from general elution problem [27] - it cannot achieve optimal separation power with both small and large ions simultaneously. Though voltage sweep method [27] has proved to be effective for solving this problem, however, the major disadvantage is also the long scanning time. SMPSs also require several minutes to complete voltage scans [24]. So these instruments are not effective for detecting the rapidly varying aerosol particles at the time of sampling with an aircraft, near roadways, or from a combustion engine. Furthermore, DMAs require the use of high sheath flow rates as well as high voltage scanning which increases the operational cost too [28]. Also, The separation of particles in a regular Drift tube spectrometers proportional to the length and electric field. To achieve high resolution (>100), the instrument length must be on the order of meters or make use of excessively high electric field [29]. However, the increased length also increase the resident time of charged particles inside the drift tube resulting diffusion broadening. The greater length, as well as higher electric field, also precludes portability of IMS instruments.

Therefore, it is needed to improve the Ion Mobility systems based on the following characteristics:

- Fast electrical mobility characterization system for rapidly varying aerosols particles
- Able to detect wide range of mobilities (0.3nm<diameter<100nm)
- A small device (length < 50cm)
- Operational in room pressure
- Can be coupled to a CPC [30] (or an electro-meter)
- Able to show high resolution by correcting diffusion broadening
- Compete against well-established DMAs

Considering all these characteristics, in this work, a new instrument concept is proposed based on the DTIMS [31] that uses two varying controllable opposite forces to correct for diffusion broadening [28]. In this instrument, the resolution is dependent on mobility which is inversely proportional to the size of the particles. This instrument has been termed as Inverse drift tube (IDT) as the electric field opposes the migration of the nano-particles, dragged by sheath gas flow [28]. Two different separation techniques- IPF (Intermittent push flow) and NSP (Nearly stopping potential) separation can be used for successful separation of charged particles following this concept.

2. ANALYTICAL AND NUMERICAL SOLUTION OF IDT

2.1 Separation Techniques Using Inverted Drift Tube

In an inverted drift tube the separation mechanism is as follows: At room pressure, packages of ions of multiple mobilities, is inserted at the entrance of the tube which is controlled by an ion-gate pulsing mechanism- high voltage prohibits the ion to pass through the gate, and low voltage permits ion to enter the tube. Ions that enter are then pushed by a gas flowing with a velocity v_{gas} downstream [28].

A series of electrodes are equally spaced inside the drift tube and are connected through resistors into a power supply. The electrodes are used to create a linearly increasing electric field which opposes the flow of the ions and slow their movement relative to v_{gas}. This allows the ions to be separated depending on their mobility through the drift velocity v_{drift}. As the field opposes the flow, the lowest mobility ions or bigger ions are the ones moving ahead in contrast to a regular DT-IMS hence the term Inverted has been used. Figure 2.1 shows the sketch of an Inverted Drift Tube with the gas flow direction and opposing field. As long as the ratio v_{drift}/v_{gas} , termed from here on separation ratio, Λ, is smaller than unity, the ions of a given mobility will traverse through the drift cell without being completely stopped. Eventually, these ions can be collected downstream of the drift tube. The closer $\Lambda = v_{drift}/v_{gas}$ is to 1, the longer time the ion remains in the drift cell and the higher the separation will be. However, if at some point inside the drift cell, the ratio $\Lambda = 1$ is reached, particles of such mobility would be stopped and pushed towards the walls due to the residual radial electric field that arises from Laplaces equation where $\Delta^2 V = 0$ [28]. One good way to confine ions inside the Drift tube is to use RF. TIMS (Trapped Ion Mobility Spectrometry) [13,32,33], the most recent IMS instrument, uses this kind of mechanism for trapping ions [32]. However, it only works in low-pressure condition.

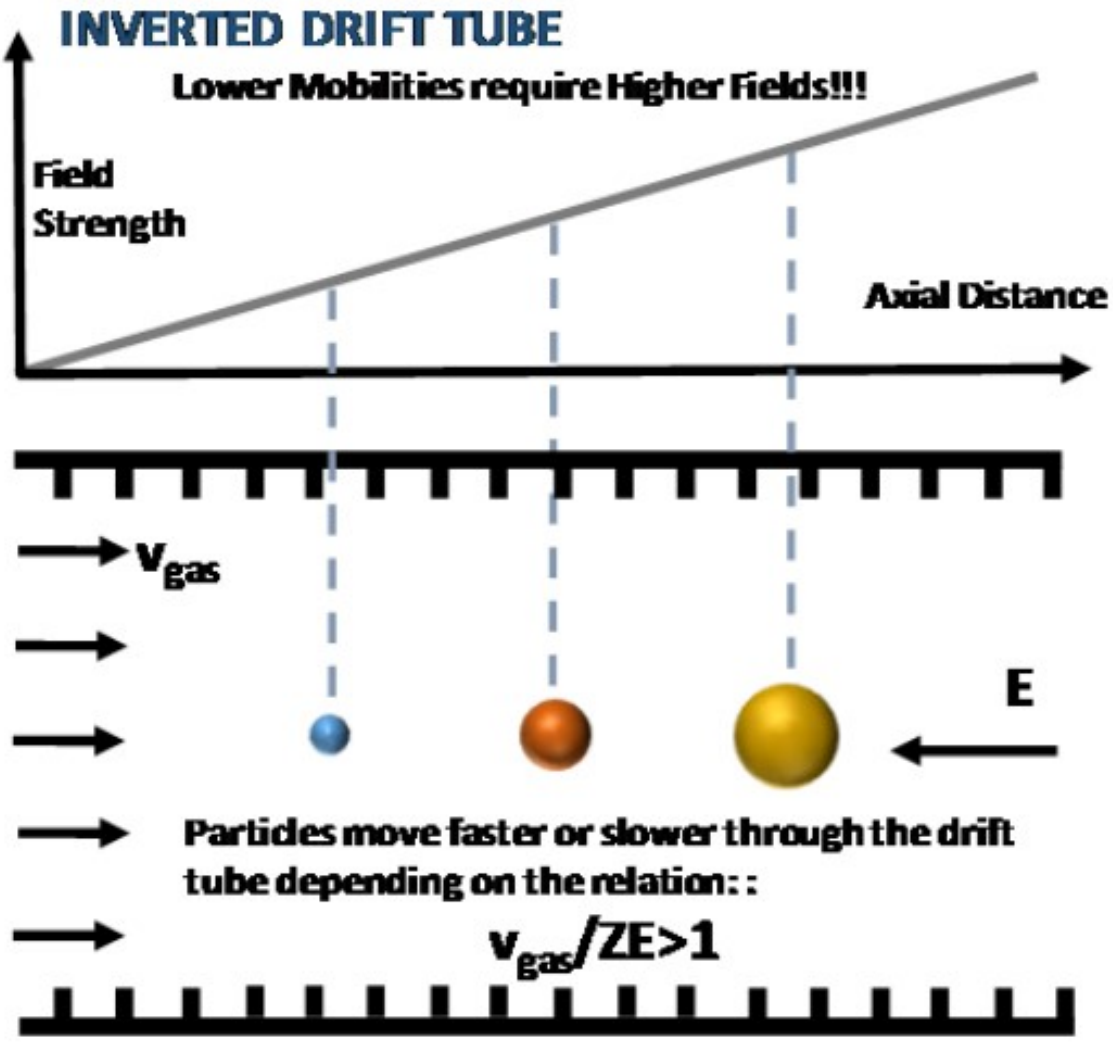

Figure 2.1. Inverted Drift Tube System. The gas flow in the direction of the moving ions and the linearly increasing electric field in the opposite direction

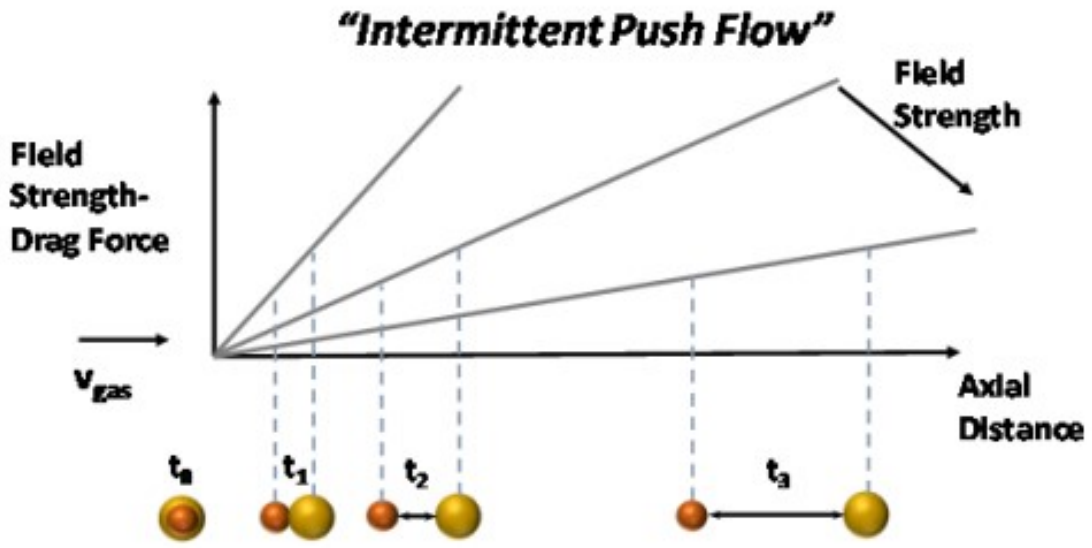

Figure 2.2. Intermittent push plow separation

For trapping relatively bigger ions, the RF would have to be very high in amplitude and frequency which is difficult to pursue.

The alternate idea can be to allow all mobilities of interest to traverse the drift cell while trying to keep the ratio Λ as close to 1 as possible without losing the ions. However, it is not possible to maintain the constant separation ratio under a fixed rising electric field. To illustrate more clearly, in case of separating a particular ion with a separation ratio 0.9 under fixed rising electric field the separation ratio at the beginning is zero. Separation ratio gradually increases towards the downstream side, and before reaching the end, it should achieve 0.9. For the ions with size more than the selected ion of choice separation would be either low or not possible. With that in mind, two different separation mechanisms have been explored using IDT [28]:

1. Intermittent Push Flow (IPF) Separation:

   To separate a wide range of mobilities, the varying the opposing electrical field is necessary to acquire all mobilities at high resolutions. The method is depicted

in figure 2.2 where the highest possible field slope $dE/dx = A$ for a given electrical supply is initially selected. Before the ion with the smallest mobility hits a separation ratio of Λ, the slope of the electric field is lowered which ensures that $\Lambda = 1$ will never be reached. This drop in the slope can happen as many times as needed until all necessary ions are collected at the end of the drift tube. The resolution and separation of the peaks will depend on the range of mobilities. Figure 2.2 shows, two ions of different sizes at the entrance of an IDT as well as the initial electric field at starting time t_0.With time the electric field gradually decreases and maximum separation occurs at time t_3.

2. Nearly-Stopping Potential (NSP) Separation :

   To separate ions of very close mobilities, an alternative possibility is to use an opposing constant electric field which is slightly below the necessary field to maintain the separation ratio slightly below 1 for all ions of interest hence maximizing the separation potential. To avoid the radial electric field as well as trap ions inside an RF of low amplitude and low frequency also can be used in this technique. Figure 2.3 shows, at time t_1 ions face the constant rising electric field, and at time t_2 the electric field is made constant, and separation occurs.

Based on the range of mobilities and the resolution either IPF or NSP can be used. The advantage of these type of opposing-field instruments is their auto-correcting properties- from equation 1.1 if the electric field strength E is less than the ion drift velocity v_{drift} then ions will be pushed forward, and if the opposite is true, then ions will be pushed backward.

The major difference in between IDT and TIMS is, in IDT the separation ratio $\Lambda < 1$ always for particular ions of choice, however, in TIMS ions reach separation ratio, $\Lambda = 1$ and then one RF field is used to trap ions in the different location based on their mobilities [28].The ions are then subsequently pushed by lowering the electric field to the critical value that pushes the particles through. On the other

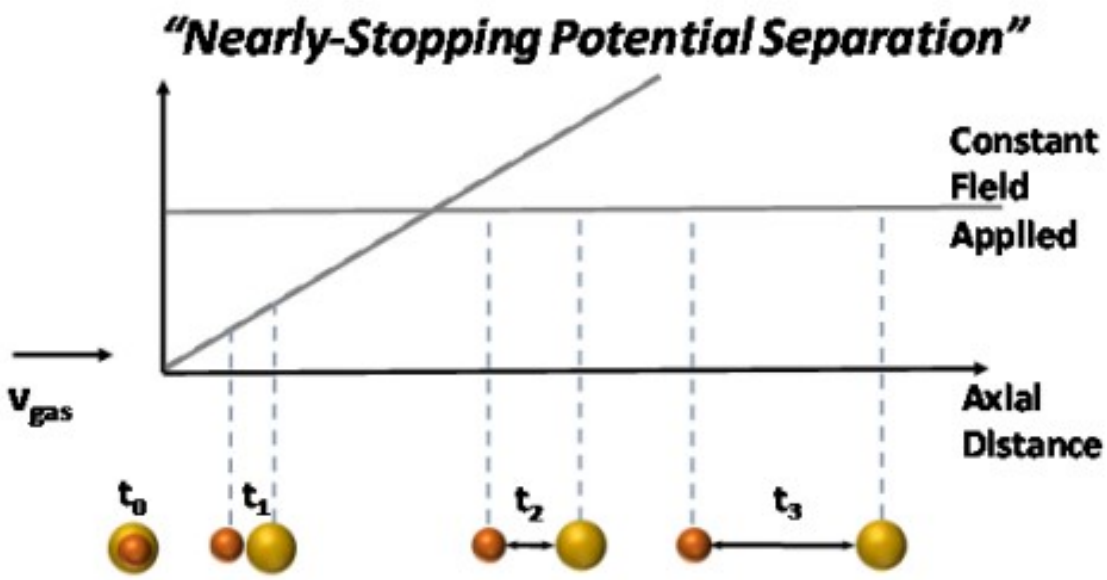

Figure 2.3. Nearly Stopping potential separation

hand, in IDT, the electric field is continuously decreased without any influence of RF to maintain the constant separation ratio.

2.2 Analytical Solution of IDT

The differential equation and corresponding solution are already established for typical drift tube and thereby, the resolutions of those of drift tubes are also predictable. On the other hand, as the concept of IDT is quite new, so, It is needed to find the proper differential equation and the solution of that to represent diffusion auto-correction.

To avoid complexity, we can assume that the IDT has a fixed increasingly linear electric field $\vec{E} = A\vec{z}$, is applied opposite to the gas flow at a velocity v_{gas}. A is the slope of the field. The study can be made more simpler considering the concentration of $n(r, z, t)$ ions of a particular mobility K and charge q drift inside the tube. And, the concentration of ions $n(r, z, t)$ is low enough so that the effect of space charge can be neglected.Then the balance equation can be represented as:

$$\partial n/\partial t - \Delta.(\bar{\bar{D}}.\Delta n - (\vec{v_{gas}} - K\vec{E})n) = 0 \tag{2.1}$$

$\bar{\bar{D}}$ is the diffusion tensor and K is electrical mobility. If one considers the one-dimensional problem neglecting radial electric field and diffusion, the equation for $n(z, t)$ can be written in Cartesian coordinates as:

$$\partial n/\partial t = D_L(\partial^2 n/\partial x^2) - (\vec{v_{gas}} - KAz)\partial n/\partial z) + KAn = 0 \tag{2.2}$$

The initial concentration of ions at the inlet of the tube and at time t_0 can be considered $n(0, 0) = n_s$

The Sturm-Liouville solution to the equation for the aforementioned initial concentration can be written as [28]:

$$n(z, t) = n_s/\sqrt{2\pi\sigma^2}\exp^{-(z-\vec{x})^2/2\sigma^2} \tag{2.3}$$

where,

$$\begin{aligned}\sigma^2 &= (2D_L/v_{gas})(\bar{x} - KA/2v_{gas}\bar{x}^2) \\ &= (D_L/KA)(1 - exp^{-}2KAt) \\ &= (KT/qA)(1 - e^{-2KAt})\end{aligned} \tag{2.4}$$

and

$$\bar{x} = (v_{gas}/KA)(1 - e^{-KAt}) \tag{2.5}$$

There are several characteristics that differentiate this equation from that of the regular drift tube. Most importantly, the standard deviation σ as shown in equation 2.4 has a correction term $KA/2v_{gas}\bar{x}^2$. This auto-correction term is quadratic with the mean position $\bar{x}$ of the distribution so that it increases with the traversing distance through the drift cell. While in the conventional Drift Tube distribution broadens as a function of time, in the IDT distribution broadening is damped and eventually stopped. The contribution of $KA/2v_{gas}\bar{x}^2$ increases with time, and as the ion advances through the drift cell, leads to an asymptotic value of the standard deviation given by kT/qA which is independent of time t. This asymptotic value will be reached when the separation ratio Λ becomes one. At that moment, the mean position of the distribution will be given by, v_{gas}/KA and the ion will no longer advance in the axial direction.

The resolution for the IDT can also be calculated as [28]:

$$R = \bar{x}/\Delta x = (\bar{x}/2)/\sqrt{2\ln 2(KT/qA)(1 - e^{-2KAt})} \tag{2.6}$$

The resolution of a typical DT of Length L is known as [29]:

$$R_{DTIMS} = \bar{x}/\Delta x = tv_{drift}/\sqrt{16D_L t\ln 2} \tag{2.7}$$

Where, D_L is the longitudinal diffusion. For IDT, the resolution at distance L can be calculated as [28]:

$$\begin{aligned}R_L &= L/\sqrt{16\ln 2(KkT/qv_{gas})(L - KA/2v_{gas}L^2)} \\ &= \sqrt{qL}/\sqrt{16\ln 2(KkT/qv_{gas})(1 - KA/2v_{gas}L)} \\ &= R_{DTIMS}/\sqrt{\Lambda(1 - \Lambda/2z)}\end{aligned} \tag{2.8}$$

2.3 Results from Analytical Solution

2.3.1 Resolution Using Varying Opposed Field (Intermittent Push Flow Separation)

The equation 2.6 is representing that the resolution in IDT varies with distance travel inside the drift tube. With time the numerator term $\bar{x}$, which represents the mean position of a particular particle, increases and the denominator term $\sqrt{2\ln 2(KT/qA)(1-e^{-2KAt})}$ decreases. The contribution of both ultimately makes the resolution much higher on the downstream side. It should be noted here that, in both IDT as well as typical DT the resolution increases with the length of the drift tube. Equation 2.7 shows the term tv_{drift} which is ultimately the length L in proportion to the resolution for regular DT. From the equation 2.8, the resolution for inverted drift tube is equal to the resolution of regular drift tube divided by the term $\sqrt{\Lambda(1-(\Lambda L/2z))}$. Figure 2.4 shows the resolution as a function of Length and different mobilities (8-80 nm diameters particles) for a fixed slope A and v_{gas}. It can be mentioned here that, unlike the resolution of the DT depicted in equation 2.7, the resolution of the IDT has a positive dependence on the mobility. The resolution of the instrument is very high in terms of equation 2.8 for very modest lengths (12 cm). From figure 2.4, the resolution increases with increasing diameters or decreasing mobilities, however, under constant electric field condition the separation ratio is not different for different particles. Figure 2.4 shows when 8nm diameter particles gradually increase to a separation ratio close to 1 then 80nm diameter particles reach to a separation ratio $\Lambda < 0.01$ at the end of the conduit.

To improve the resolution and separation ratio, one must resort to the tactics IPF and NSP separation discussed earlier. For the intermittent push flow, there is a theoretical optimal resolution for which the separation ratio Λ is kept constant for a particular mobility. This requires the continuous change of the field slope A to guarantee that at any given position of the ion Λ *constant*. Figure 2.4 shows the theoretical resolution maximum (dashed lines) for 80nm particles as a function

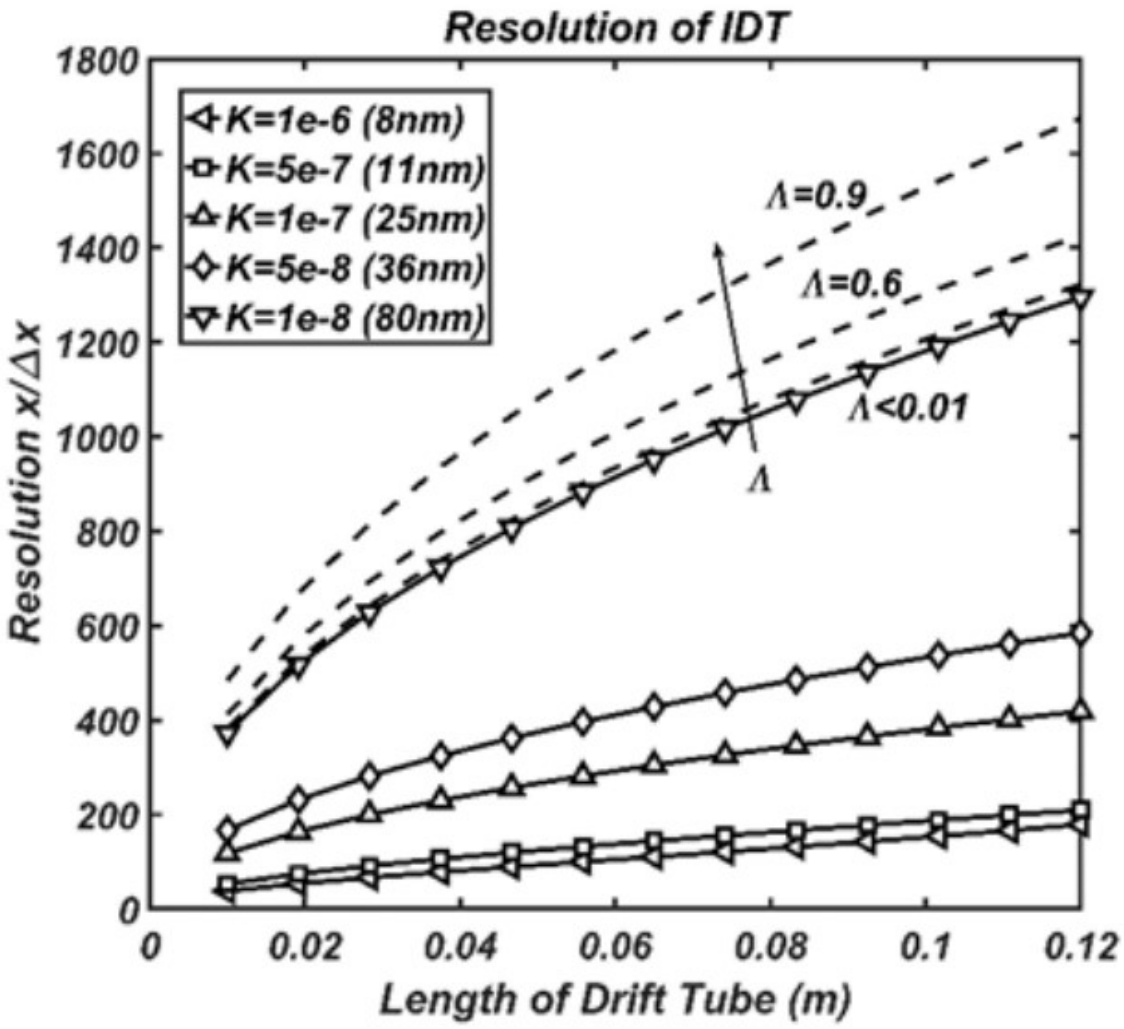

Figure 2.4. Mobility dependent IDT resolution for $v_{gas} = 0.04m/s$ and $A = 3.25e5V/m^2$

of the different constant values of the separation ratio. The resolution, as given in equation 2.8, is not particularly useful for this type of instrument as opposed to the DMA or DT-IMS. The reason is that if the field slope was A=0, i.e., no electric field, the residence time in the drift tube will be minimal and there will be no separation between any mobilities. However, the resolution would depend on the competition between diffusion and V_{gas} which could still be very high. The importance of equation 2.8 relies on the fact that when the separation ratio Λ increases, the residence time inside the system increases, but the resolution also increases in contrast to what is expected with just diffusion.

Since the electric field is solenoidal when space charge is neglected, the radial electric field might be non-negligible off axis, and one must wonder about its effect in the trajectories of the ions as the separation ratio is increased [28]. Given, $\Delta.\vec{E} = 0$ one can calculate the radial field for constant axial field cross sections $\partial E_z/\partial z = -A$ and which is given by $E_r = Ar/2$. Figure 2.5 shows the trajectories of off-axis particles due to the effects of radial electric fields (no diffusion considered) for two particular cases:

1. For constant separation ratio condition where electric field needs to decrease continuously. Figure 2.5 shows for constant separation ratio $\Lambda = 0.5$ (dashed lines) the trajectory of 8 nm diameter particles mobility, $K = 1 \times 10^{-}6m^2/Vs$. The initial condition was 2.4 cm as the slope A would be too high to maintain a constant separation ratio Λ for smaller values of z. It is found that values that are off axis up to 1.1cm still reach the end of the tube.

2. Constant slope condition where the separation ration is no longer constant. The separation ratio Λ increases with the distance z progressively reducing the velocity of the moving ions $V_m = V_{gas} - V_{drift}$ until the drift from the radial field becomes of the order of V_m at a given radial position. If this occurs, the ion will inevitably be lost.

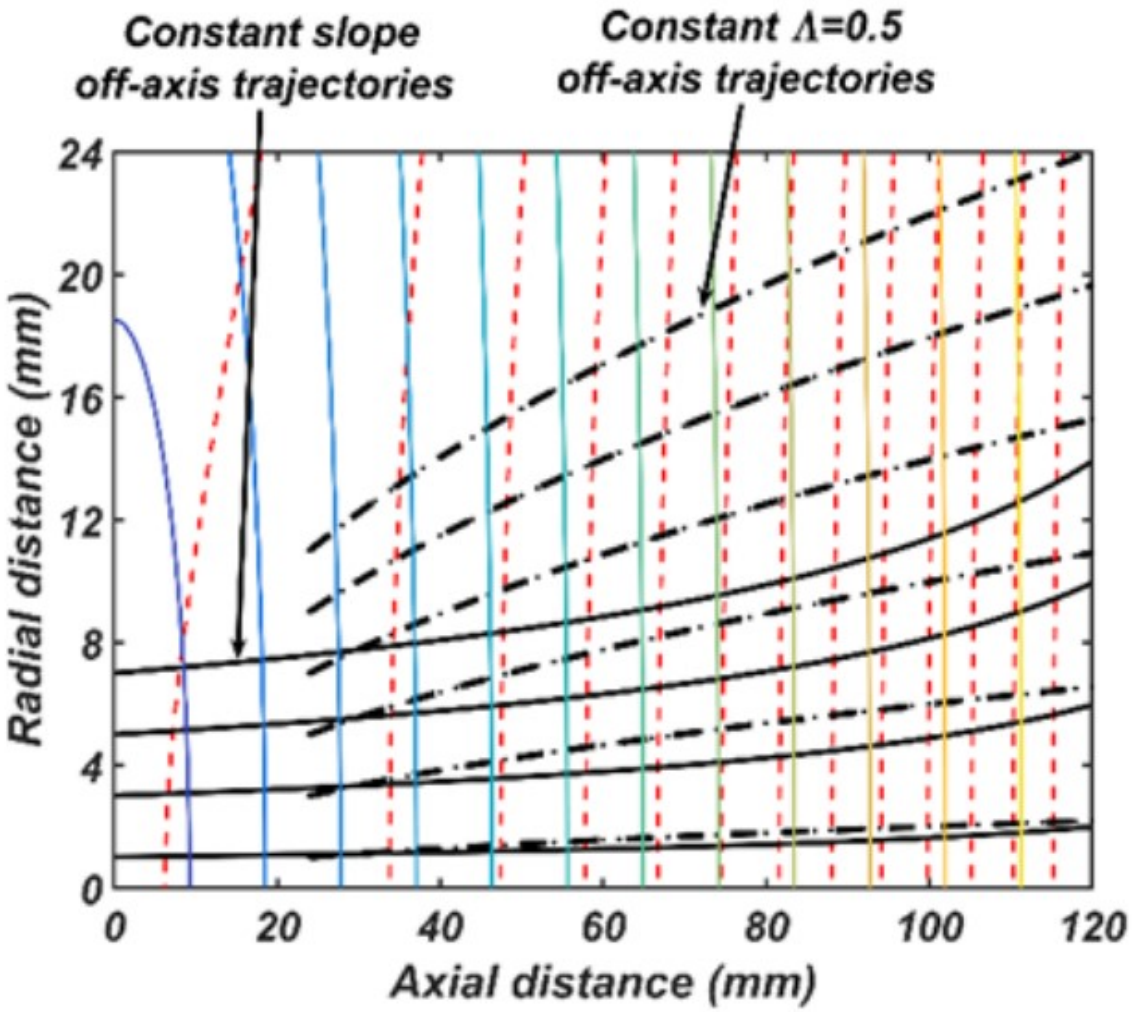

Figure 2.5. Off axis trajectories due to the existing radial field in Intermittent Push Flow. Perpendicular lines to the axial direction are iso-field lines (color-map) and iso-potential lines (dashed red) for a constant A. Solid black lines correspond to off axis trajectories at different initial radial conditions using Intermittent Push flow for constant slope A. Dotted black lines correspond to trajectories at a constant separation ratio Λ.

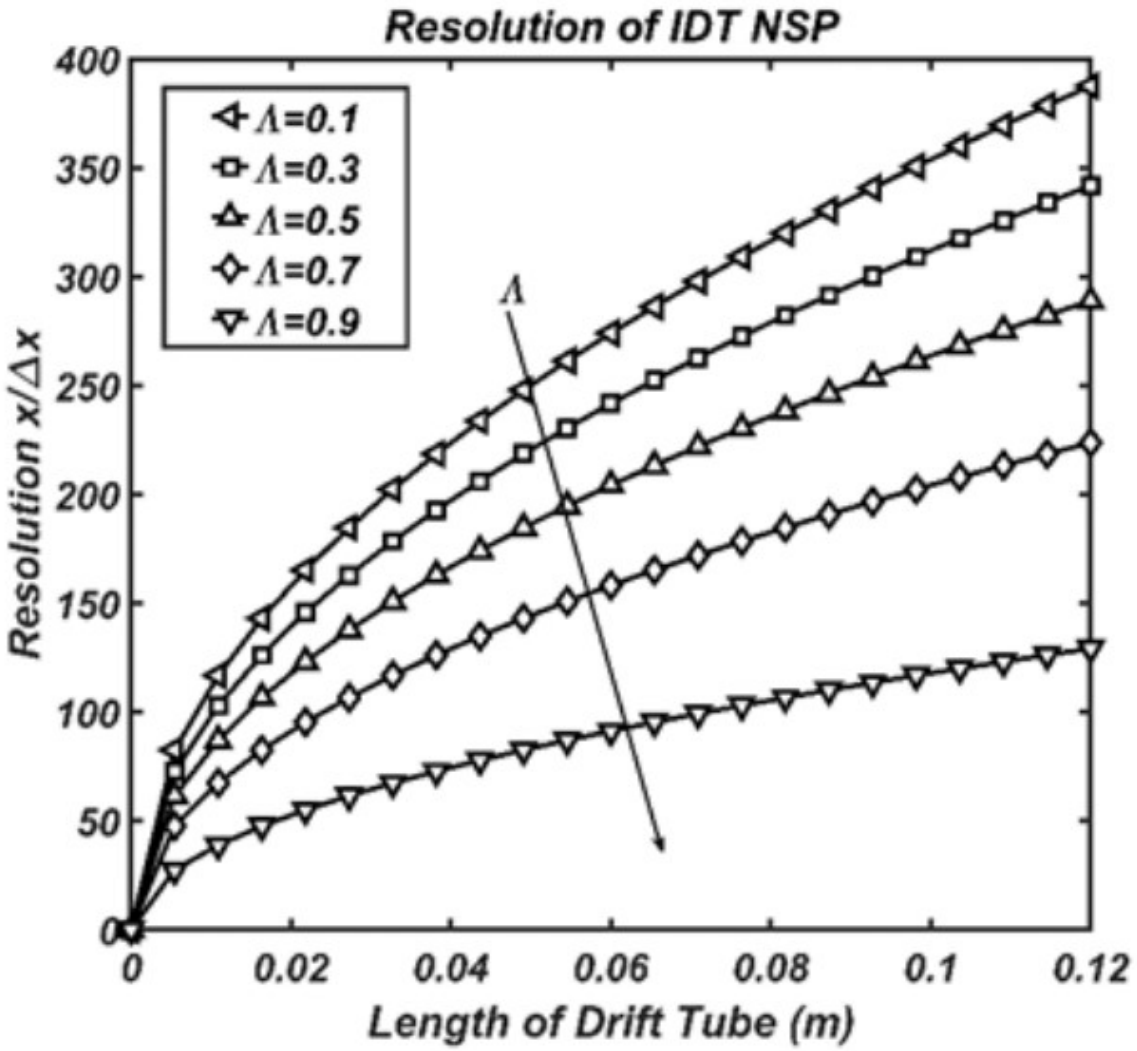

Figure 2.6. IDT resolution using the Nearly-Stopping Potential (NSP) method.

2.3.2 Resolution Using Constant Opposed Field (Nearly-Stopping Potential Separation)

To avoid radial field effects, one can resort to NSP separation mode where the electric field is constant. For such a case, the resolution R_{NSP} of a distribution of ions of mobility K after passing through the cell is equivalent to that of a DT-IMS from equation 2.7 but where the field opposes movement [28]:

$$R_{NSP} = \bar{x}/\Delta x = \sqrt{qlv_m/16kT\ln 2K} = \sqrt{qlv_{gas}(1-\Lambda)/16kT\ln 2K} \tag{2.9}$$

It is very important to note here that, the separation ratio opposes the resolution. The reasoning is quite clear, the larger the separation ratio, the longer the total residence time in the drift tube and the higher the chance ions have to diffuse (similar to that of the regular drift tube) before covering a distance L. Figure 2.6 shows the resolution for nearly stopping potentials for a given mobility $K = 1 \times 10^{-}7m^2/Vs$ (25nm) as a function of the separation ratio where it is showing with increasing the separation ratio the resolution is decreasing.

2.4 Numerical Simulations Including Diffusion Auto-correction

The 1D numerical solution of equation 2.8 shown in figure 2.7 where the position of the distribution of singly charged ions of a single mobility is given as the function of time for a specific set of parameters, namely A, K, v_gas, D_L and initial condition $n_s(x)$. The advantage of using numerical methods is that one can easily use the initial condition to be a distribution n_s of any kind at time $t = 0$ and study its evolution. In figure 2.7, there are a couple of notable features. The first of them is that there exists a maximum value of x at which the distribution of ions reaches an asymptotic behavior. This asymptotic behavior happens, as stated previously,

$\bar{x_{asympt}} = v_{gas}/KA$ and it will occur when the separation ratio reaches the value of 1. The second is that the standard deviation of the ions will also asymptotically tend to value $\sigma_{asympt} = kT/qA$ regardless of the initial distribution. To test whether

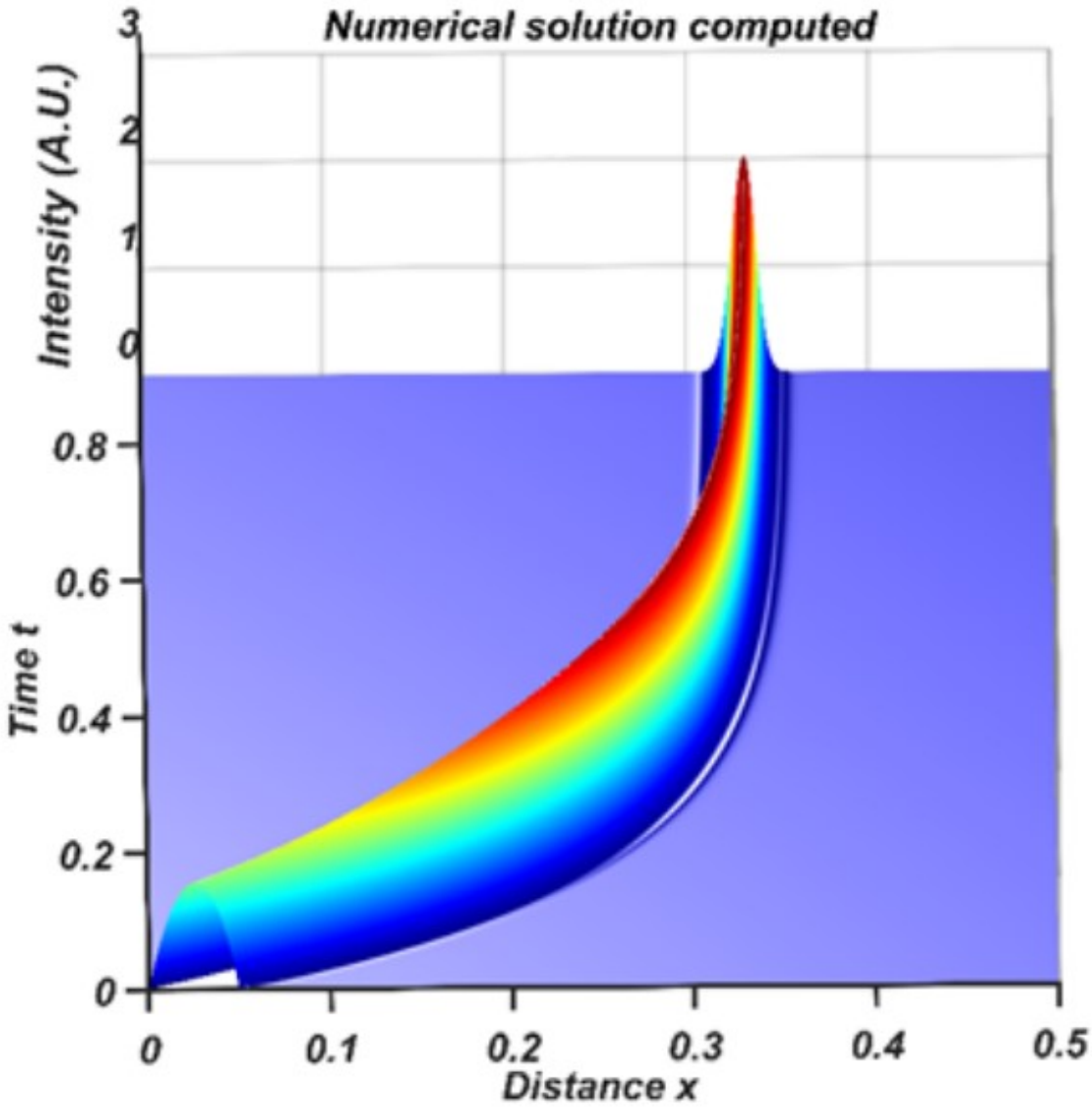

Figure 2.7. 1D numerical solution for equation 2.8 showing the position of the distribution as a function of time for an initial broad parabolic distribution.

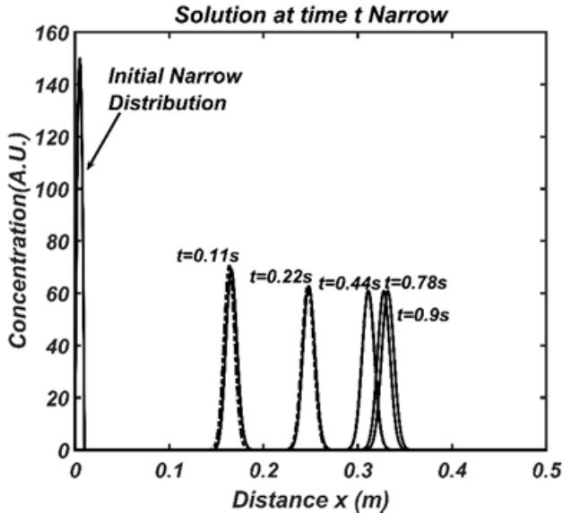

Figure 2.8. Simulation of the 1D IDT equation 2.8 at different times. Dashed lines correspond to the analytical solution equation 2.3 while solid lines correspond to the numerical solution at times t=0 s,0.11 s,0.44 s,0.78 s and 0.9 s for initial narrow distribution.

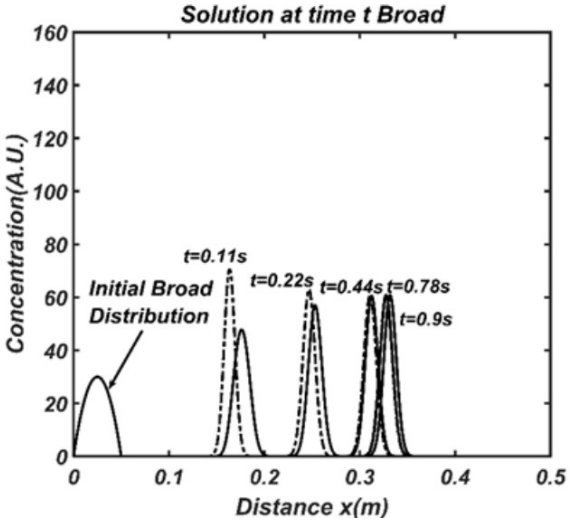

Figure 2.9. Simulation of the 1D IDT equation 2.8 at different times. Dashed lines correspond to the analytical solution equation 2.3 while solid lines correspond to the numerical solution at times t=0 s,0.11 s,0.44 s,0.78 s and 0.9 s for initial wide distribution.Diffusion auto-correction is able to narrow down the initial distribution as it travels through the drift cell.

the asymptotic standard deviation was reached from different initial distributions, two initial distributions were modeled; one with smaller standard deviation than the asymptotic value $\sigma_{initial} < \sigma_{asympt}$) and one with a larger one $\sigma_{initial} > \sigma_{asympt}$. The distributions as a function of time are shown in Figure 2.8 and 2.9, and both are compared to the analytical solution -obtained using equation 2.3 giving excellent agreement between numerical (solid) and analytical (dashed) distributions. Figure 2.8 clearly shows that when the initial distribution is very narrow, the distribution broadens and reaches the expected asymptotic behavior. The behavior follows the analytical solution quite accurately. When the initial distribution is broader than the expected asymptotic solution as in Figure 2.9, the distribution narrows to reach the expected asymptotic solution. This behavior is unique to the IDT instrument and provides the possibility of ultra-high resolution if we allow the ions to stay in the cell for a sufficient length/time. The reasoning behind the auto-correction of the diffusion broadening is quite apparent. Ions diffusing to the left of the equilibrium point have values of $\Lambda < \Lambda_{eqilibrium}$, and are pushed forward faster than those at $\Lambda_{eqilibrium}$.Similarly, for those ions diffusing to the right, $\Lambda < \Lambda_{eqilibrium}$ and they suffer a stronger electrical field which subsequently pushes them back to equilibrium [28].

3. SIMULATIONS IN SIMION

3.1 SIMION and Collision SDS Model

SIMION is an ion optics simulation software package that can model ion optics problem with 2D symmetrical and 3D asymmetrical electrostatic potential arrays. Based on different generated 2D or 3D shapes and applied voltage, SIMION can generate the virtual electric fields or magnetic fields. It also consists of ion characterization options according to need. Ions can be flown from the different positions inside or outside the generated electric field-and trajectory of the ions are calculated by the finite difference numerical scheme. It is also possible to define any flow field inside SIMION to mimic the actual flow of gas. The unique feature of SIMION is, almost any command can be feed in SIMION through LUA programming language.

As for application, SIMION is suitable for a wide variety of systems involving 2D or 3D for static or low-frequency (MHz) RF fields. It is capable of doing simulation from ion flight through simple electrostatic and magnetic lenses to particle guns to highly complex instruments including time-of-flight, ion traps, RF quadrupole, ICR cells, Mass Spectrometry, ion source and detector optics.

SDS (Statistical Diffusion Simulation) is a user program for SIMION that simulates the motion of charged particles in electrostatic and magnetic fields under atmospheric pressure [34,35]. SDS uses collision statistics to simulate the effect of millions of collision per unit time step [34, 36, 37].

3.1.1 Parameter Specification in SIMION

In SIMION for SDS model it is needed to define some parameters beforehand including the collision gas mass (in nm), collision gas diameter (in nm), pressure (in torr), temperature (in kelvin), bulk gas velocity (in m/s) in x,y and z-direction,

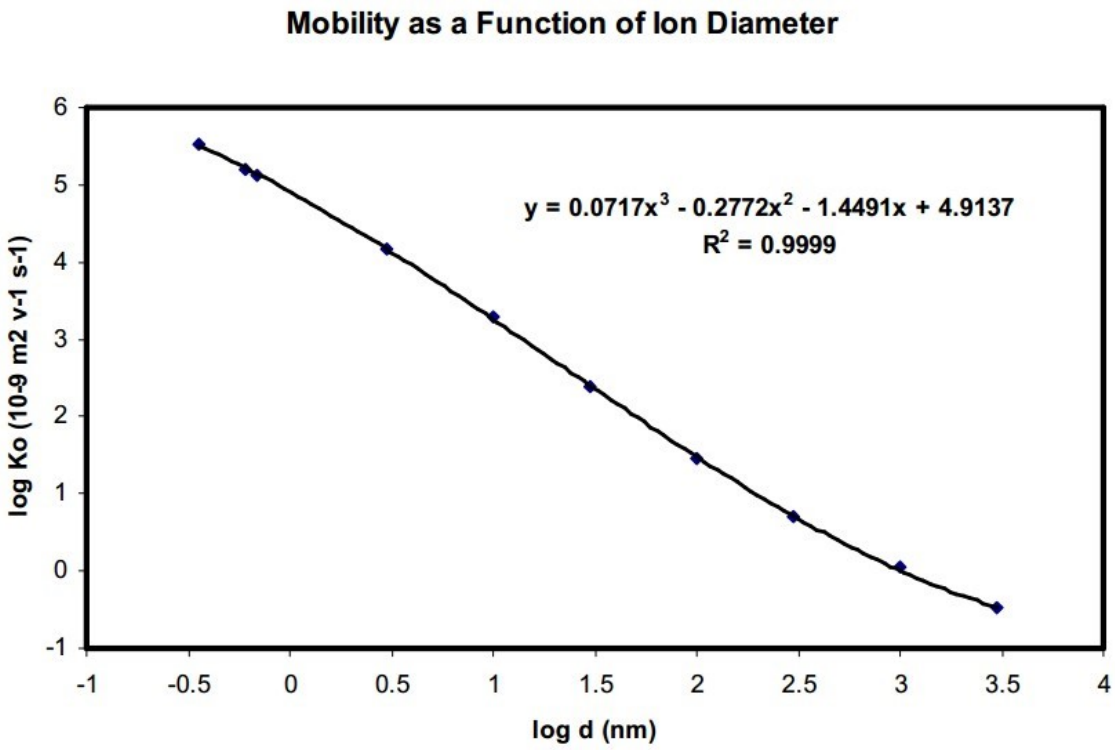

Figure 3.1. Mobility as function of ion diameter.

pressure field and Temperature field, velocity field and minimum time step. If no data are provided by the user regarding the mobility and collision diameter for ions to fly then, SIMION automatically estimates them for simulation.

Ion Diameter, Mass and Mobility

SIMION uses the following formula for estimating the diameter of ion if the ion mass is provided with an assumption of constant volume density (from atmospheric aerosols 14-35 Handbook of Chemistry and Physics 83rd edition):

$$d_{ion}(nm) = 0.120415405(mass_{ion}(amu))^{1/3} \tag{3.1}$$

If the mobility is not provided, then it can be generated by fitting log-log plots of ion diameter and mobility values in the air (from page 14-36 The Handbook of Chemistry

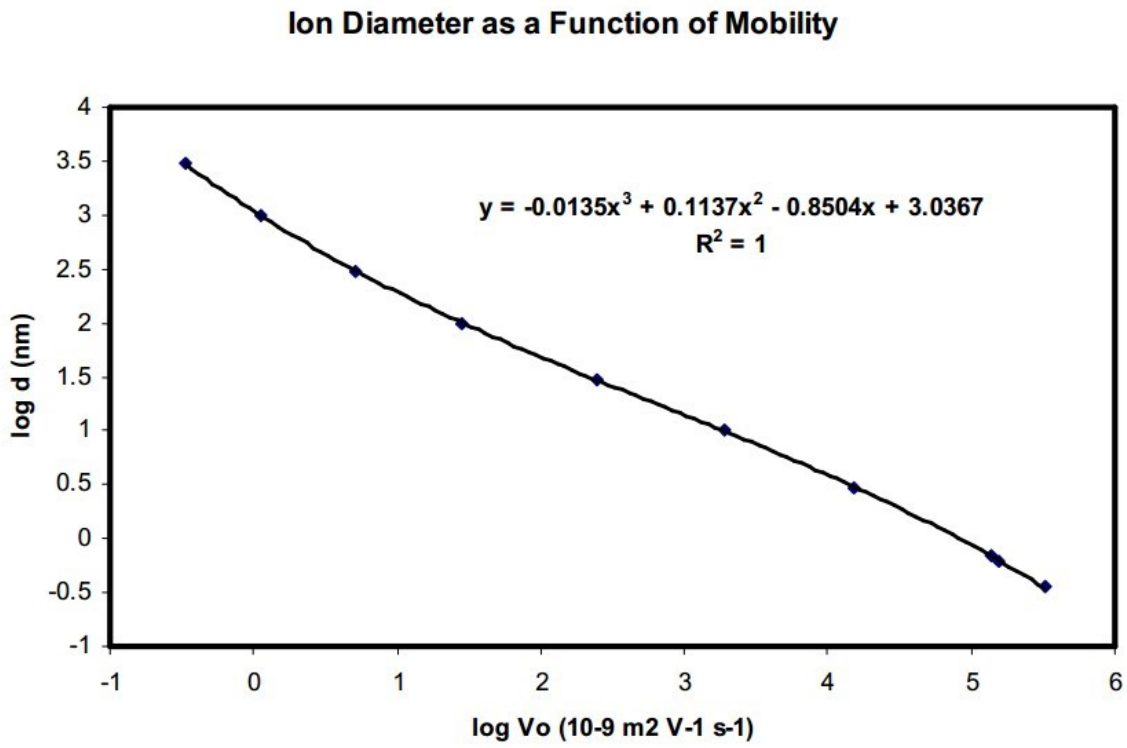

Figure 3.2. Ion diameter as function of mobility.

and Physics 83rd edition) using a third order polynomial. Figure 3.1 shows the log-log plot for mobility as the function of diameter and the following relation as the polynomial equation.

Before calculation starts, some other parameters are needed to be configured in SIMION. They are:

Position, Kinetic Energy and Distribution of Ions

In a separate tab in SIMION it is needed to provide the initial position of ions, number of ions, kinetic energy as well as initial distribution. Figure 3.3 shows the ion configuration options in SIMION.

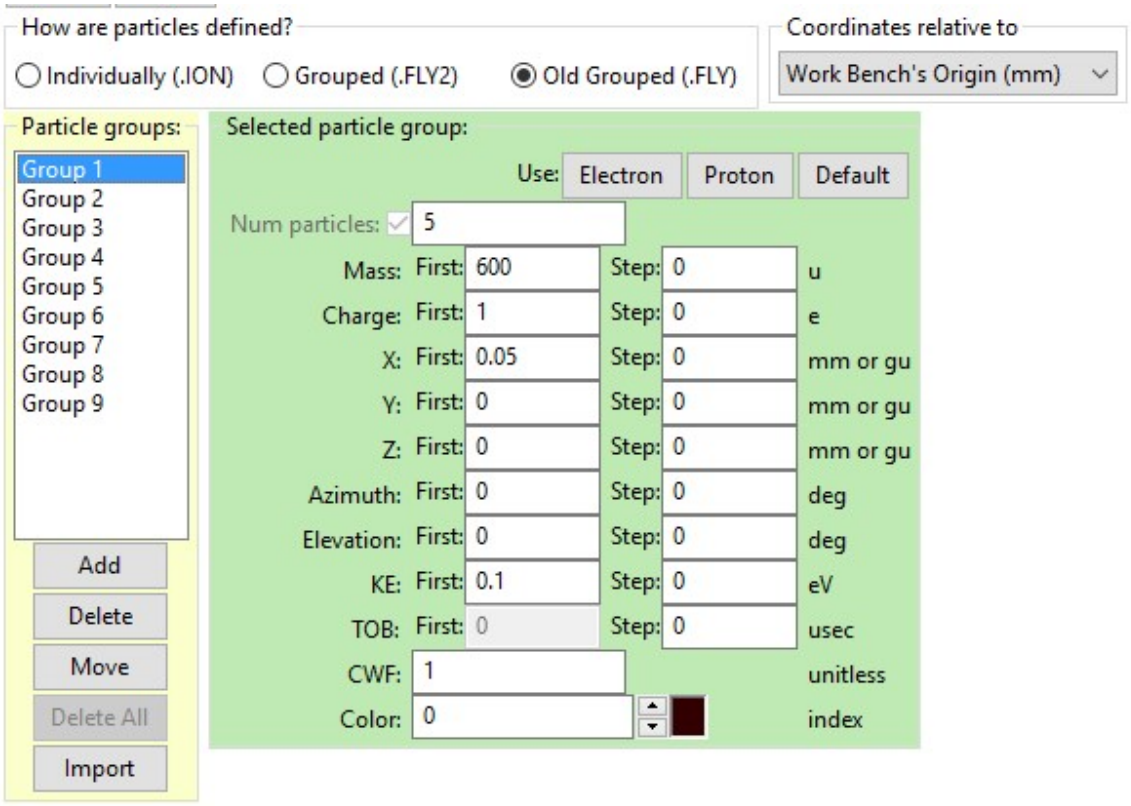

Figure 3.3. Ion Definition in SIMION

Buffer Gas Mass and Diameter

By default, SIMION assumes air as buffer gas (mass = 28.954515 atomic mass unit (amu) and diameter = 0.366 nm). If the buffer gas is not air then the ions diameter and and the mobility are calculated from the equation of gas kinetics [35]:

$$K_0 = 3e/16N_0((2\pi/\mu kT)^{1/2})(1/\Omega) \tag{3.2}$$

Where μ is the reduced mass and Ω is collision cross section. They can be defined mathematically as:

$$\mu = (mass_{ion} \times mass_{gas})/(mass_{ion} + mass_{gas}) \tag{3.3}$$

$$\Omega = \pi(d_{ion} + d_{gas})^2/2 \tag{3.4}$$

The mobility of gas k_{0gas} and mobility of air k_{0air} are estimated at standard temperature and pressure as follow:

$$k_{0gas} = k_{0air} * C_{gas/air} \tag{3.5}$$

$$k_{0air} = k_{0gas}/C_{gas/air} \tag{3.6}$$

where,

$$C_{gas/air} = (\mu_{air}/\mu_{gas})^{1/2}(\Omega_{air}/\Omega_{gas}) \tag{3.7}$$

$$C_{gas/air} = (\mu_{air}/\mu_{gas})^{1/2}((d_{ion} + d_{air})/(d_{ion} + d_{gas}))^2 \tag{3.8}$$

So, if the diameter of ion d_{ion} is known but mobility of ion in gas K_{0gas} is unknown then using the mobility of ion in air K_{0air} (can be found from fitting equation at figure 3.1) mobility of ion in gas K_{0gas} can be calculated from equation 3.5. On the other hand, if mobility of ion in gas K_{0gas} is known, but, the ion diameter d_{ion} is unknown then at first using the mass of ion the diameter of ion can be calculated from equation 3.1 and next, mass and diameter of ions can be used to calculate $C_{gas/air}$, which later can be utilized to find the mobility of ion in air K_{0air}. Knowing the mobility of the ion in air K_{0air} from equation 3.2 the actual diameter of ion can be calculated.

Velocity, Pressure and Temperature Field

In SIMION the velocity and pressure, temperature values are either can be kept constant throughout the simulation time or, the velocity, pressure and temperature field can be provided in each grid point defined in SIMION. The values of velocity, pressure, and temperature can be provided as the text file.

Electric Field

In SIMION, at first, 3D geometric figures are to be drawn in the grid specified. The 3D geometry can be declared as electrodes or non-electrode. SIMION calculates the electric field based on the electrode geometry, empty space and the potential applied to that electrodes. Potentials in that electrodes either can be provided externally or by using an LUA program in SIMION. Figure 3.4 shows the generated grid points as well as electrodes in SIMION. Figure 3.5 shows the 3D electrodes generated by the geometry presented in Figure 3.4.

3.1.2 Statistical Diffusion Simulation (SDS) Calculation Method

In SDS collision model at the atmospheric pressure, the ion motions are simulated by a combined viscous ion mobility x_{axial} and random ion jump r_{jump} calculation which is again the function of the number of collisions of ions with gas molecules. Collision statistics are used for simulating the high number of collisions per unit time steps. In collision statics, it is assumed that any particular ion can move to a random distance at random direction from any initial point due to a fixed number of collisions for a particular mass ratio. The mass ratio is the ratio between the mass of the ion to the mass of the gas molecule. A distribution of random movements of ions can be found considering a large number of ions (e.g. 1,000,000) with different mass ratios as well as the different number of collisions.

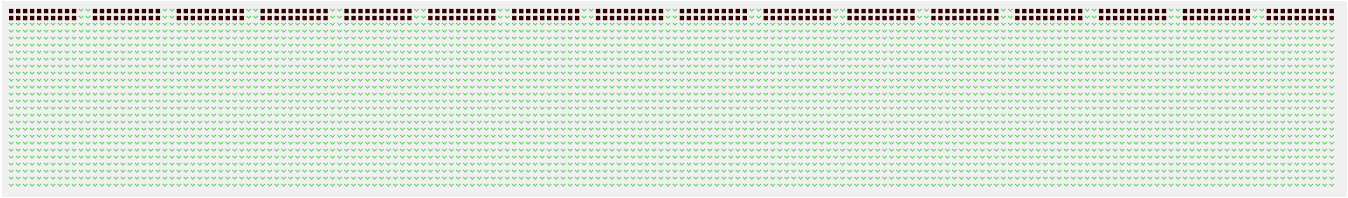

Figure 3.4. Grid points (green) and Electrode (Khaki color) generated in SIMION

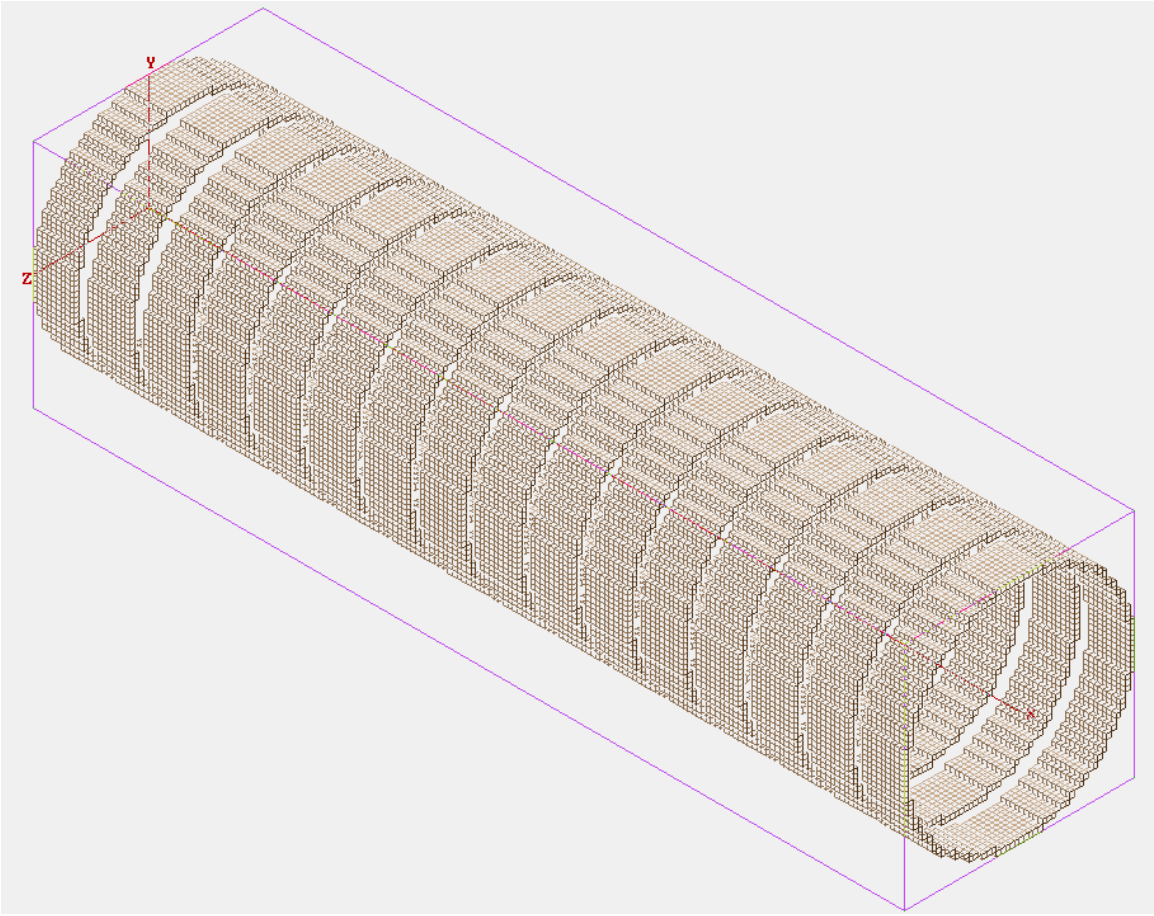

Figure 3.5. 3D Electrodes generated by the drawing presented in Figure 3.4

The process of can better be explained considering the following two collections of simulations: the first collection of the simulation considered ion with the normalized velocity of 1 along x-axis and a normalized fixed distance step of 1. The second simulation used random Maxwell Boltzmann distribution of energy (average normalized to 1) and direction, and each distance step was Poisson randomized to an average of 1 (normalized). Each simulation was done for 10000 ions. A separate simulation was run for each of five different total number of collisions (10, 100, 1000, 10000, or 100000), and had one of seven mass ratios (1, 10, 100, 1000, 10000, 100000, or 1000000). Thus each collection had 35 simulations. The figure 3.6 shows a comparison of the variation of the 50% r distribution point for these simulations. The most important observation is that both collections with the equivalent mass ratios converge to common r (50%) values when the number of collisions is large enough. This means that both approaches lead to the same r statistics for large values of n collisions. Also, it is notable that, the lower mass ratios converge at a lower number of collisions, n. Any ion jumps r_{jump} for a particular mass ratio, in between calculated mass ratios, can be found using interpolation. These random movements can be superimposed upon the viscous trajectories to predict the more realistic movement of ions. In figure 3.6 the graph leads to the insight that, if the number of collisions is high enough (around 100000), the mass ratios of less than 10000 to 1, converge into the square root law. This means that if the time steps are large enough for 100,000 collisions, we can ignore the linear rule region and assume the ion trajectories will be fully de-correlated and fly in the square root law scaling region. This condition is easily satisfied for ions flying in atmospheric conditions using the sub to one mm integration steps typically used by SIMION.

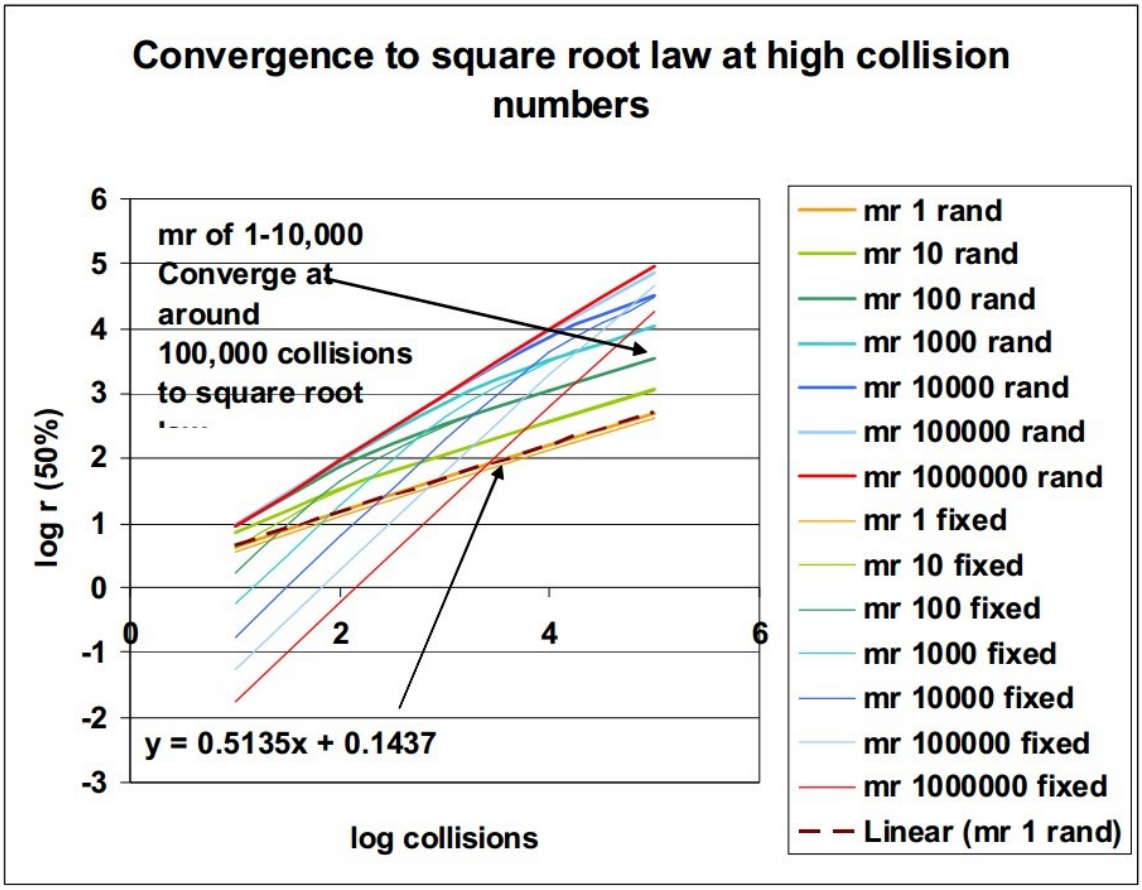

Figure 3.6. Convergence to square root law at high collision numbers.

3.1.3 Formulations of SDS Collision Model

Formulations for Random Jump:

The number of expected collision $n_{expected_collisions}$ of ions with the gas molecules can be found from the following equation [35].

$$n_{expected_collisions} = t\bar{V_{ion}}/MFP \tag{3.9}$$

Where $\bar{V_{ion}}$ is ions average thermal speed, and MFP is mean free path of ions and t is time step. Ions average thermal speed can be calculated from:

$$\bar{V_{ion}} = \sqrt{8kT/(\pi m_{ion})} \tag{3.10}$$

The mean free path between collisions is found by dividing the average thermal velocity of the ion $\bar{V_{ion}}$ by its collision frequency ν_{rate}.

$$MFP = \bar{V_{ion}}/\nu_{rate} \tag{3.11}$$

Where,

$$\nu_{rate} = (\sqrt{2} - 1/4)\pi((d_{ion} + d_{gas})^2/2)N\bar{V_i}on + \pi d_{ion}^2 N v_{gas}/4 \tag{3.12}$$

Where, N is the number density of the gas, V_{gas} is the velocity if gas, d_{ion} and d_{gas} are the diameter of ion and gas molecule respectively.

The true ions jump $r_{jump-scaled}$ can be found from [35]:

$$r_{jump-scaled} = MFP \times r_{obtained}\sqrt{n_{expected-collision}/n_{dist-collision}} \tag{3.13}$$

For a particular mass ratio in between two known mass ratios, the particular true ion jump $r_{obtained}$ is found via interpolation from two sets of distribution for those known mass ratios. $n_{dist-collisions}$ is the number of collisions calculated from that distribution. This random movement of ion in the random direction is repeated at each time step throughout the ions trajectory and superimposed over the viscous movement to find the actual movement.

Formulations for Viscous Movement:

The mobility (either from the user or calculated from ion diameter) is used for calculating the viscous movement of ion inside gas. Considering the damping effect of ion in a buffer gas, the acceleration of an ion can be found as [35]:

$$A = A_0 e^{-b_0 t} \tag{3.14}$$

Where, A_0 is the initial acceleration, b_0 is time constant and A is the acceleration at any time t. Integrating the equation 3.14 we get the velocity

$$\int_0^t A_0 e^{-b_0 t} dt \tag{3.15}$$

or,

$$V = A_0/b_0(1 - e^{-b_0 t}) \tag{3.16}$$

From this equation 3.16 the term $(1 - e^{-b_0 t})$ decreases with time and the ions eventually attain the maximum velocity V_0. Where,

$$V_0 = A_0/b_0 \tag{3.17}$$

This maximum velocity V_0 is directly related to the mobility by following equation:

$$V_0 = K_0 E = K_0 * Volts/distance \tag{3.18}$$

Where K_0 represents mobility and E represents electric field. The acceleration term can also be written as,

$$A_0 = force/mass = work/(distance \times mass) = (Voltage \times charge)/(mass \times distance) \tag{3.19}$$

Using this value from equation 3.18 we get

$$A_0 = (charge \times Volts)/(mass \times distance) \tag{3.20}$$

Therefore, using the value of A_0 from equation 3.16 we can write,

$$b_0 = charge/(mass \times K_0) \tag{3.21}$$

The time constant includes damping coefficient inside and damping is inversely proportional to the mobility. Therefore, it can be written:

$$b_0 \propto 1/K_0 \tag{3.22}$$

This time constant b can be corrected for any local pressure and temperature in the following way [35]:

$$b = b_0(P_{local}/P)(T/T_{local}) \tag{3.23}$$

So, knowing in each time step using the velocity of ion V (from equation 3.16), the axial movement of the ions is calculated from:

$$x_{axial} = V \times timestep \tag{3.24}$$

Where, V is the velocity of ions at local temperature and pressure.

In SIMION, this random ion jump r_{jump} is then superimposed to this axial viscous movement x_{axial} to calculate the actual movement distance and direction at any specific ion time of flight. For the next time step, SIMION considers these calculated values as initial values and the previous end-location of ions as the stating location and continue calculating the trajectories until all the ions reach the end. Altogether, figure 3.7 represents the flow chart for input parameters and calculated values considering SDS collision model in SIMION.

3.2 Simulation of IPF and NSP Separations Using SDS Collision Model

After finding the analytical solution for IDT concept, the validity of this system was also checked by SDS collision model. Inside SIMION, 30 ring electrodes each of 48 mm inner diameter, 50 mm outer diameter and 2 mm thickness were drawn in 121×25 grid points (the distance in between any two grid points was 1mm). The space in between two consecutive ring electrodes was kept 2 mm for the spacers. The target was to separate the wide range of mobilities ranging from 20 nm to 120 nm. By using an LUA code, the potentials of the ring electrodes were set in such a way that

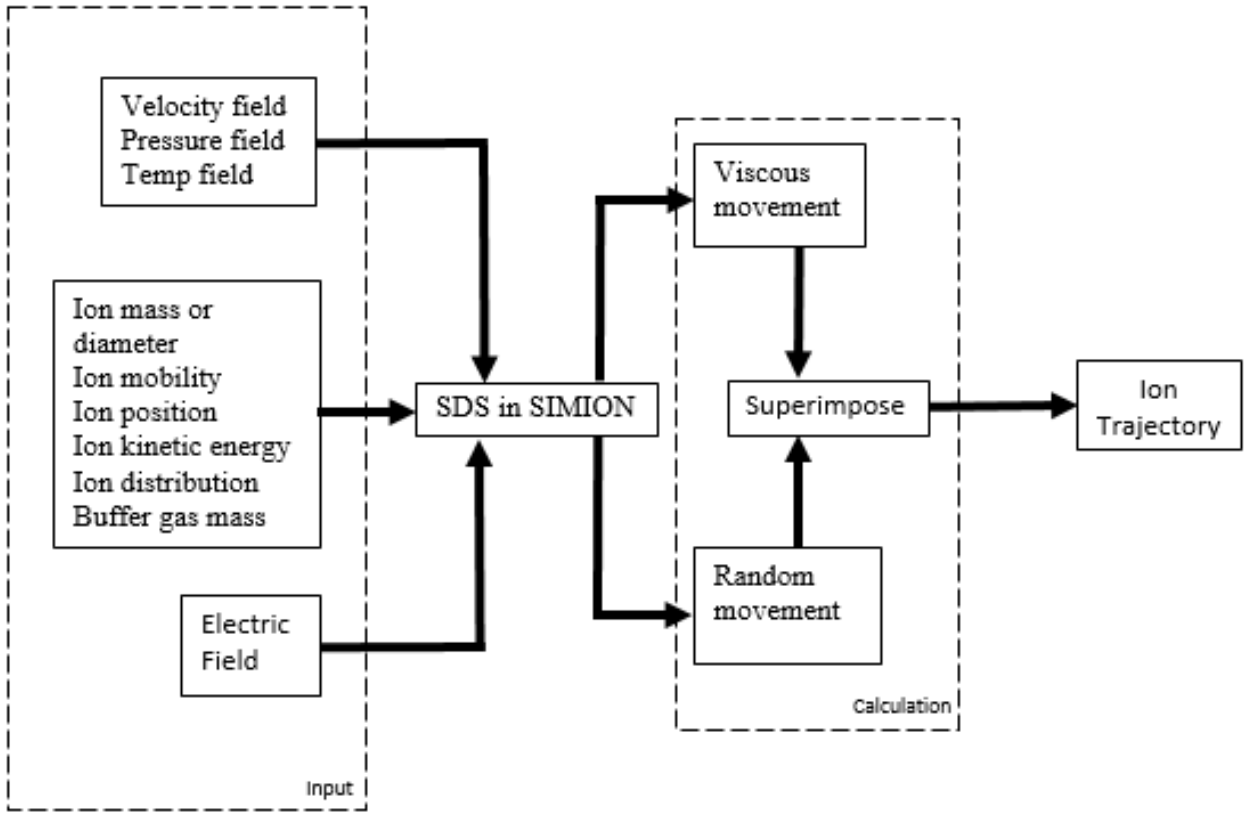

Figure 3.7. SIMION flow chart for input parameters and calculated values using SDS collision model

they follow a quadratic relation with distance: potential, $V(n) = Ax^2$, where A is an arbitrary constant and x represents the distance. It is because the potentials then form linearly increasing electric field towards the downstream side. The equation of electric field becomes E= $dV/dx = 2A$, where, $2A$ represents the slope of the electric field vs distance graph in figure 3.8. Figure 3.8 a) shows a section of the IDT with simulated electric field lines (blue) and b) shows the expected potential and electric field inside IDT including the slope $2A$ of the liner electric field. However, It can be noted here, the electric field lines were not perfectly linear (figure 3.8 (a)) rather, slightly curved due to the presence of radial electric fields which were unavoidable. The existence of this radial field caused the ions (with separation ratios Λ close to 1) to be pushed towards the electrodes precluding the possibility of capturing the particles inside the drift tube. To avoid reaching separation ratios very close to 1, the two techniques (mentioned in Chapter 2) were developed: Intermittent Push Flow (IPF) and Nearly-Stopping potential (NSP) separation and were run in SIMION.

In order to define a reliable gas flow field, a CFD simulation of the drift tube using Solid Works flow simulation was performed. A CAD model was prepared according to the aforementioned dimension of the conceptual IDT (inner diameter 48 mm and length 120 mm). In the CAD model, two inlet-one for ion flow with air (low flow) and another for annular air flow (high flow) and one outlet were generated for CFD calculation. The center flow 1L/minute and annular flow 4L/minute were considered for CFD simulation. The outlet condition was environmental pressure.

One of the biggest problems of IMS instrument was the parabolic flow profile. In case of the parabolic profile, the similar-mass ions can be at the different position over the parabolic profile, thereby, hampers the resolution. In case of making the flow profile less parabolic or flat one mesh structure was installed both at the inlet and outlet section of the CAD model. Figure 3.9 shows the SolidWorks CAD model, inserted mesh at both inlet and outlet as well as the flow profile at the different position of the drift tube. The flow data from the CFD simulation was then transferred to SIMION as a .txt file. The two most important observations from the simulation

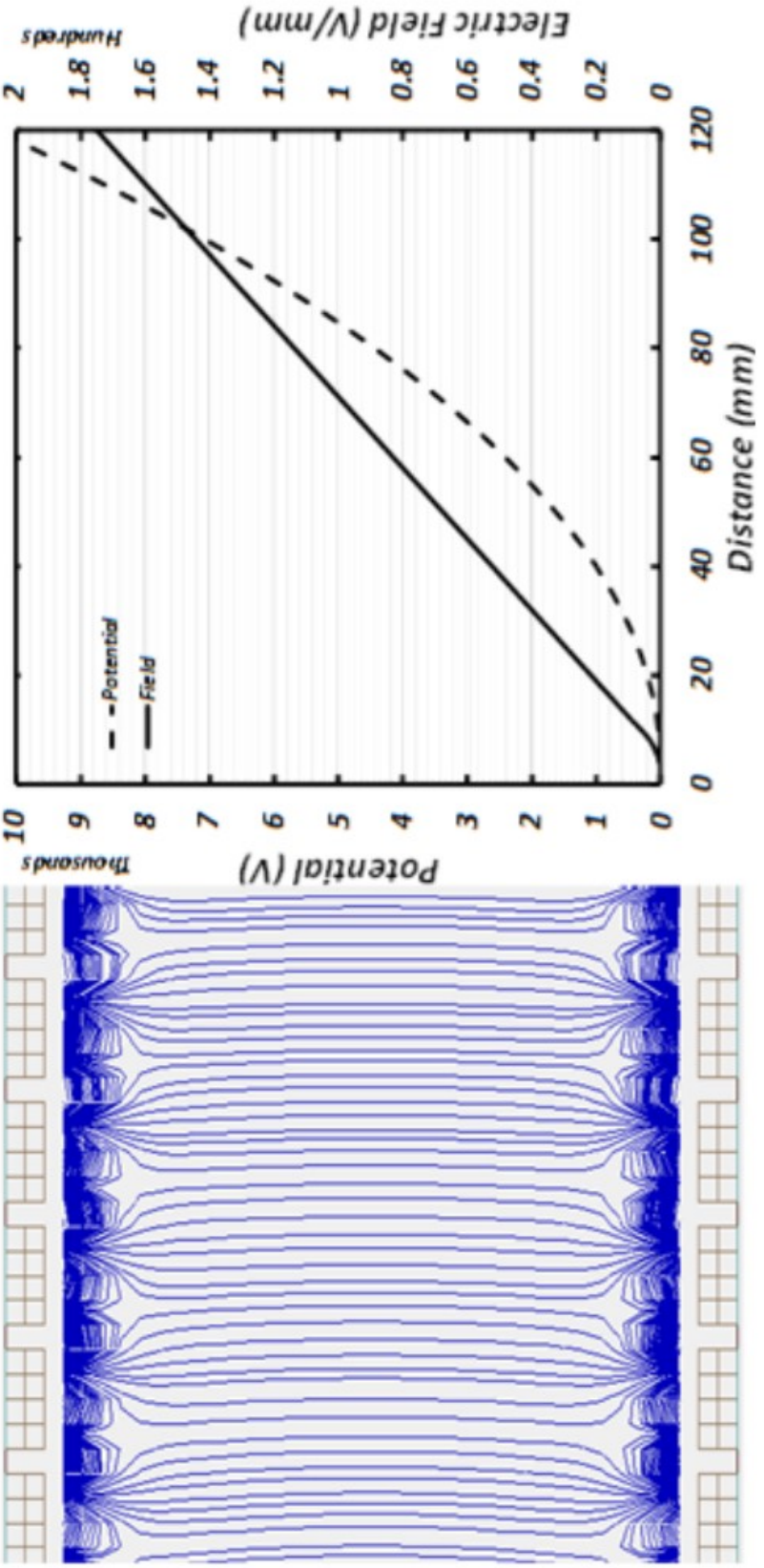

Figure 3.8. a) Schematic of the IDT. Constant electric field lines are shown for convenience (blue). b) Expected axial voltage and field due to the electrodes.

Table 3.1. Table of selected ions' mass, diameter and mobility

Mass (amu)	Diameter (nm)	Mobility (m2/Vs)
5.00E+06	20.59	5.40E-07
2.00E+07	32.69	2.35E-07
6.00E+07	47.14	1.22E-07
1.00E+08	55.93	9.03E-08
2.00E+08	70.42	6.03E-08
3.00E+08	80.61	4.77E-08
5.00E+08	95.57	3.56E-08
1.00E+09	120.42	2.41E-08

were, the flow velocity in the mid-section of the drift tube increased towards the downstream side, and at the same time, the flow profile was flat at the mid-section. Inside SIMION eight types of particles (of different masses and diameters) were defined for flying through the drift tube under the calculated electric field and provided flow field. The particles chosen are shown in table 3.1. The starting coordinate of the ions was chosen (0.5, 0, 0) in mm in the Cartesian coordinate system. No Kinetic energy was provided to ions.

3.2.1 Intermittent Push Flow Simulation in SIMION

In intermittent push flow approach the field slope $2A$ was lowered at known fixed times so as to never reach a separation ratio of Λ=1. Figure 3.10 shows a SIMION simulation at 5 particular times using the modeled spherical nano-particles of 8 different sizes ranging from 20 to 120 nm as they travel through the inverted drift tube. For easy calculation, to reduce the burden of simulation as well as simulation time, instead of continuous ramping in the simulation, 4 pushes were used at 4 specific times. To optimize the pushes, the pushes were made before the separation ratio Λ

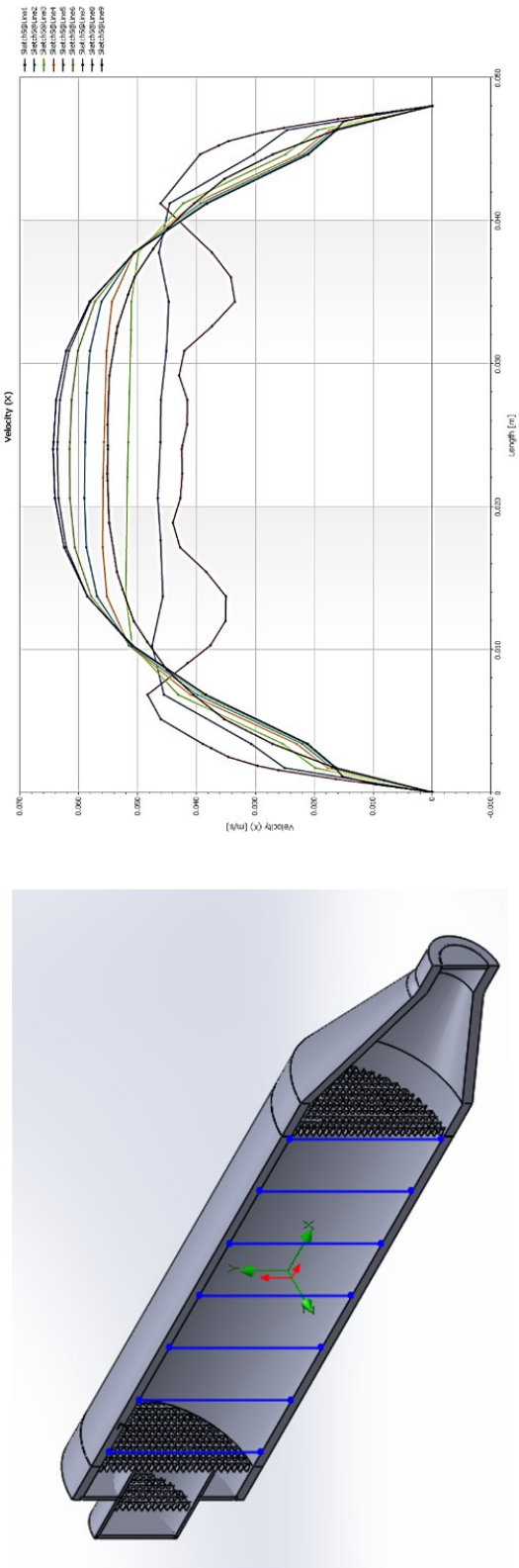

Figure 3.9. SolidWorks CAD model and flow profile

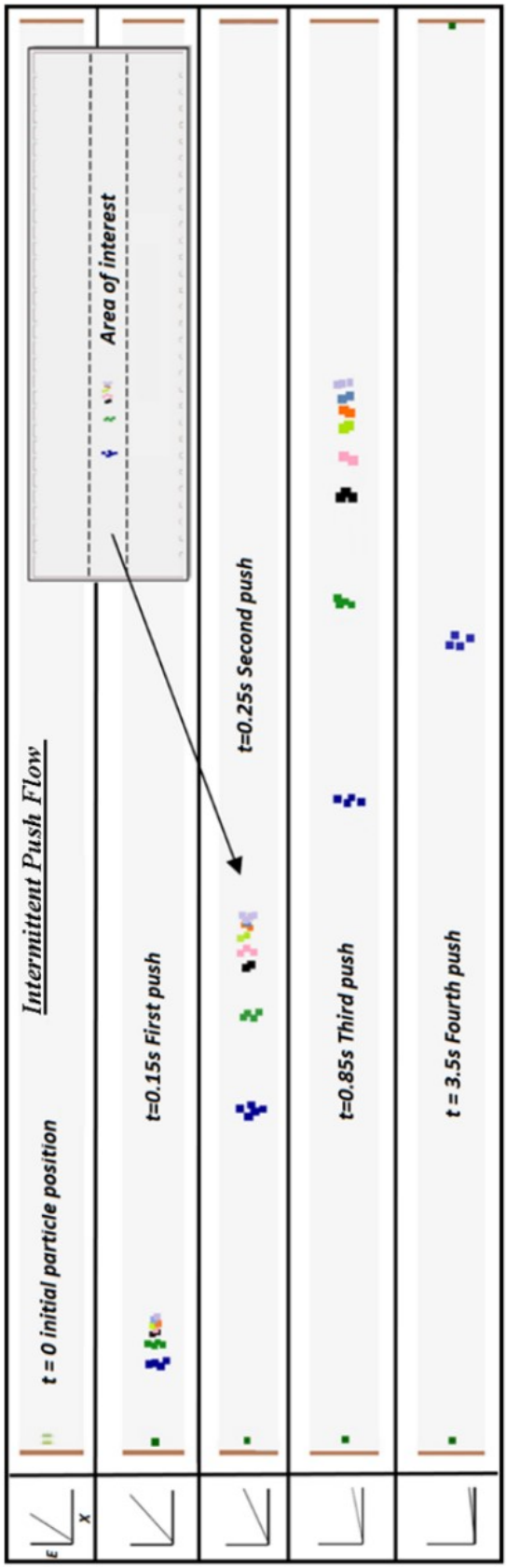

Figure 3.10. Separation of ions using IPF separation approach.

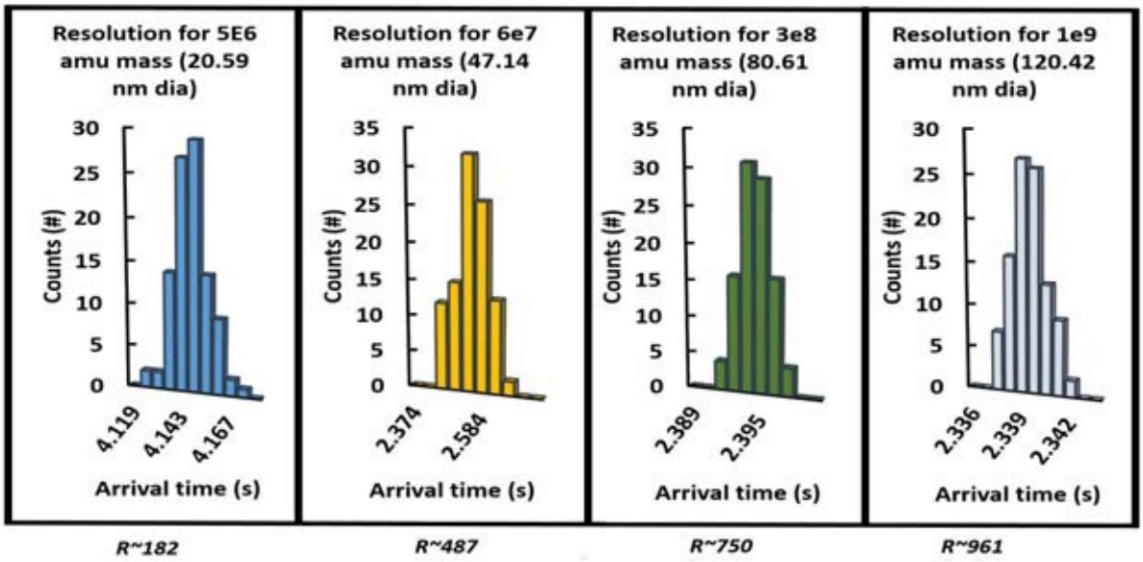

Figure 3.11. Distributions and Resolution $R\ t/\Delta t$f simulations using the set of intermittent pushes for different particles sizes. 100 nanoparticles were used to create the distributions.

became 1 for the highest mobility particle (blue in the figure). At 4 different times, specific potentials were supplied to the electrode in the simulation. The values of potentials with pushes are provided in table 3.2 and table 3.3.

The potential of electrode no. 1 was always kept 0V intentionally. In all the cases the potentials were based on the relation, $V = A(n-1)^2$ where V was the applied potential (measured in Volts), A was an arbitrary constant, and n was the number of the electrode. As potential more than 10KV was not possible and too high for an IMS instrument, so, in all the cases potentials were kept below 10KV in the simulation. To illustrate this more clearly, from the table 3.2 at no push condition the 10th potential was 9963V and after that, all the potentials were more than 10KV (following the formula mentioned above). For that reason, the 9963V value was applied for the rest of the electrodes. Similarly, it was also done for the push 2 as well as push 3. All the commands were supplied in SIMION using an LUA code. The pressure, velocity, and collision gas (air) diameter were also declared in that code. Using this

Table 3.2. Potentials at different push-times for electrode no. 2 to 24

Electrode No.	Potential (V)				
	No push	Push 1 at 0.15 s	Push 2 at 0.25 s	Push 3 at 0.85 s	Push 4 at 3.5 s
2	123	50	20	8	4
3	492	200	80	32	16
4	1107	450	180	72	36
5	1968	800	320	128	64
6	3075	1250	500	200	100
7	4428	1800	720	288	144
8	6027	2450	980	392	196
9	7872	3200	1280	512	256
10	9963	4050	1620	648	324
11	9963	5000	2000	800	400
12	9963	6050	2420	968	484
13	9963	7200	2880	1152	576
14	9963	8450	3380	1352	676
15	9963	9800	3920	1568	784
16	9963	9800	4500	1800	900
17	9963	9800	5120	2048	1024
18	9963	9800	5780	2312	1156
19	9963	9800	6480	2592	1296
20	9963	9800	7220	2888	1444
21	9963	9800	8000	3200	1600
22	9963	9800	8820	3528	1764
23	9963	9800	9680	3872	1936
24	9963	9800	9680	4232	2116

Table 3.3. Potentials at different push-times for electrode no. 25 to 30

Electrode No.	Potential (V)				
	No push	Push 1 at 0.15 s	Push 2 at 0.25 s	Push 3 at 0.85 s	Push 4 at 3.5 s
25	9963	9800	9680	4608	2304
26	9963	9800	9680	5000	2500
27	9963	9800	9680	5408	2704
28	9963	9800	9680	5832	2916
29	9963	9800	9680	6272	3136
30	9963	9800	9680	6728	3364

method and 4 pushes, all particles were collected and easily separated in the span of 4.2 seconds. However, the largest particles -those with separation ratio much smaller than unity- could not achieve its maximum possible separation. It was conceivable, however, if one were interested in resolving the largest particles, a higher separation ratio for such particles would be used, at the cost of losing higher mobility particles. For the pushes used in figure 3.10, 100 particles of each of the sizes were studied, sampled and their time distributions were collected in figure 3.11. The resolution was subsequently calculated as $t/\Delta t$ and shown in figure 3.11. The resolutions obtained are in agreement with those obtained in figure 2.4 and are extremely high compared to other instruments. Not a single particle was lost in the calculation process, so the transmission was 100%. However, the simulation normally had the starting particles initially centered in the drift tube (deviation was always less than 0.5cm) and space charge was neglected for the calculations. In any case, the loss of nanoparticles to the walls, even when space charge is considered, is not expected to be higher than that of existing commercial instruments when the initial distribution is centered (see Figure 2.4). Table 3.4 shows the mobilities and diameters of the particles used in the simulation as well as the electric field slope and the average positions of the ions when the pushes were made.

It shows only smaller particles are being pushed for the fourth time and all other particles reached the end before the fourth push. It also shows the bigger particles are keeping close distance at different pushes meaning the bigger particles are not highly separated comparing to smaller 20.59nm and 32.69 nm charged particles.

3.2.2 Nearly-stopping Potential Separation Simulation in SIMION

In SIMION, the same .LUA code was used for Nearly-Stopping potential separation. The only difference was instead of changing the electric field continuously the field was made constant after the certain period of time (for a particular type of particle). The constant field eliminates the radial field component almost entirely,

Table 3.4. X Distance traveled by Different particles at the Time of Push

Diameter (nm)	X distance traveled (mm)			
	Push 1 at	Push 2	Push 3	Push 4
	at 0.15 s	at 0.25 s	at 0.85s	at 3.5s
20.59	5.236514	7.92283	25.43225	98.1436
32.69	6.648518	9.972539	32.37745	
47.14	7.171221	10.85113	36.0375	
55.93	7.615708	11.31329	37.37791	
70.42	7.512206	11.60728	38.44837	
80.61	7.688492	11.8636	39.04178	
95.57	7.835918	11.5851	39.38994	
120.42	7.856611	11.65932	40.15078	
Slope A (V/mm^2)	6.1719	2.4864	0.9968	0.4984

and therefore separation ratios closer to 1 can be used without the risk of losing ions. Figure 3.12 shows a particular test where singly charged nano-particles of 55.89 and 55.93nm in diameter are trying to be separated (a 0.07% difference in diameter) using this method. All nano-particles with smaller diameters than 55.89nm will have separation ratios larger than 1 and will be stopped at the entrance of the tube. All nano-particles that are much larger than 55.89 will be promptly collected on the detector. As shown in the Figure 3.12, initially both particles are indistinguishable. However, as they travel through the drift tube, eventually the 55.89 nm particle is contained inside the drift tube for a longer period of time (approx. 10 s) and effectively separated from that of 55.93 nm. Even though the resolution given by equation 2.9 decreases with Λ, the ability to separate ions in time increases with residence time inside the cell. Indeed, the effective comparable resolution for a 0.07% difference to occur in a regular DTIMS is in the thousands, something unimaginable with other systems.

3.2.3 Resolution vs Resolving Power

As it is clear from the concept of Inverted drift tube (IDT) that, If the instrument is configured for a particular type of ion then only that particular ion will maintain the constant separation ratio inside the IDT and will be separated effectively. On the other hand, the ions bigger that the ion of choice will not maintain the constant separation ratio inside IDT and for very bigger particles separation ratio would be close to zero. At the same time the bigger particles, which are not being separated well, will move faster to the detectors and thereby it would possible to get very high resolution for those bigger particles in sacrifice of separation. However, the whole system can be tuned to separate any choice of particles, but sometimes it would be impossible due to the constraint for higher voltage usage. So, only the resolution is not enough to describe the instrument's performance. It is needed to check the separation in between the particles also. It was mentioned earlier, and the pushes were made for

Figure 3.12. Separation of 55.89 and 55.93 nm diameter particle using Nearly Stopping Potential Technique.

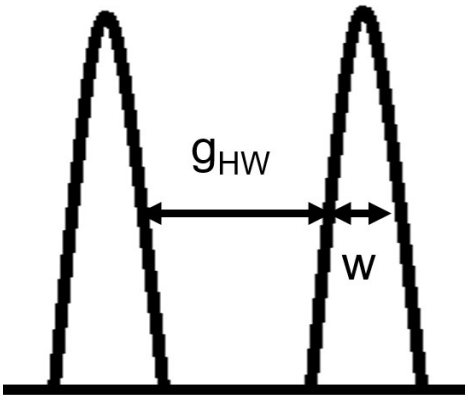

Figure 3.13. Resolving power concept

highest separation of 20.59nm particles. In another way, more separation means more resident time inside drift tube for a particular charged particle which will eventually reduce the resolution. A better option to express separation is Resolving Power, R_P given by the ratio of the gap between two peaks, at an average half maximum, g_{HW}, divided by the average width W, of the peaks. From its definition, one should expect two peaks to be resolved if $R_P < 0.1$. Figure 3.14 shows different close diameter particles resolution as well as the resolving power in a single graph. Directly from the figure 3.14, one can tell that although the resolution for the initial peaks (particle diameter of 120.42 nm and 114.47 nm) is in the thousands, the fact that the separation ratio for such ions was far from unity, provides only resolving power enough to differentiate the peaks even though, the particle diameters differed by 6nm. On the other hand, the last pair of peaks (20.59 nm and 20.93 nm), which had the separation ration Λ closest to unity, despite being only 0.34 nm apart and while having resolutions of less than two hundred. One can use the analytical resolution provided in equations 2.8 and 2.9 to provide an analytical value of the resolving Power. In such sense, R_P can also be defined as the time difference between the arrival of the center of the distribution of two similar ions divided by the average FWHM of the

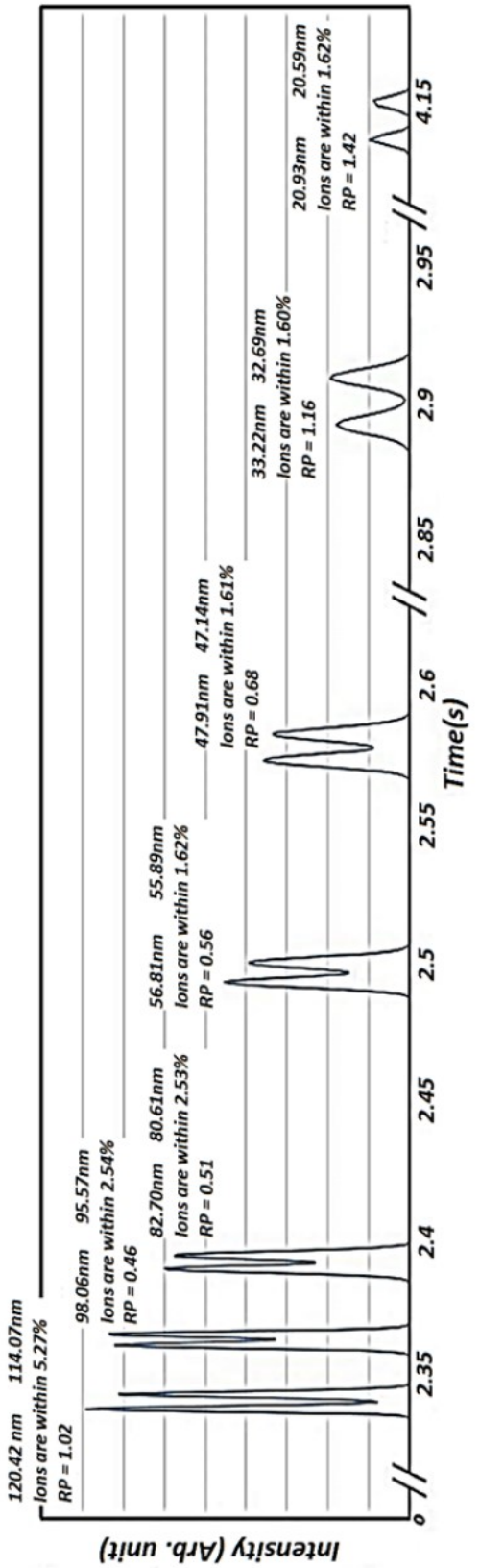

Figure 3.14. Separation of pairs of peaks using SIMION for two similar sizes. No optimization for resolution was attempted. Resolving power is used instead of resolution to specify whether or not two peaks are separable.

two peaks minus one $R_P = t_{diff}/FWHM - 1$. In particular, for IPF flow, assuming a constant separation ratio through the drift cell, the resolving power is given by [28]:

$$R_{P-IPF} = 2(t_1 - t_2)/(FWHM_1 + FWHM_2) - 1 \tag{3.25}$$

or,

$$\begin{aligned} &R_P IPF = 2\sqrt{qLv_{gas}}(1/v_{m1} - 1/v_{m2})/ \\ &(\sqrt{16kT\ln 2}(1/v_{m1}\sqrt{K_1 1 - \Lambda_1/2} + (1/v_{m2}\sqrt{K_2(1-\Lambda_2)/2}))) - 1 \end{aligned} \tag{3.26}$$

Similarly, for the Nearly-Stopping Potential Separation teh resolving power is [28]:

$$R_{PNSP} = 2\sqrt{qL}(1/v_{m1} - 1/v_{m2})/(\sqrt{16kT\ln 2}(\sqrt{K_1}/v_{m1}^{3/2} + K_2/v_{m2}^{3/2}) \tag{3.27}$$

In all cases, v_m represents the movement velocity of ions: $v_m = v_{gas} - v_{drift}$. Figure 3.15, 3.16 and 3.17 represent the Resolving power as a function of the separation ratio Λ for different scenarios. Figure 3.15 shows the Resolving Power when trying to separate mobilities that differ by 5% (2.23% in diameter) using the Intermittent Push Flow. The graphs are cut purposefully at $R_p = 0.1$ so that anything visible in the figure 3.15 can be resolved at the appropriate separation ratio. In particular, lower mobilities are readily separable for any separation ratio, while higher mobilities require higher separation ratios. For example, to separate two ions that differ in diameter 0.06nm at 2.29nm requires at least a constant separation ratio of 0.43 or higher. To understand the capabilities of the IDT, figure 3.16 shows $R_{p(IPF)}$ for nano-particles that vary between 30% and 0.1% in mobility with respect to a value of $5e^{-7}m^2/Vs(21.5nm)$. Ions are easily separable up to 1% difference (21.5nm to 21.61nm) or less. However, to be able to separate a 0.01% one would require constant separation ratios of over 0.8. Due to the existing radial field, a separation ratio this high would most likely lead to the loss of the ions before reaching the end of the drift cell [28]. In order to be able to use higher separation ratios, the nearly-stopping potential can be used (in figure 3.17). The first thing to notice between figures 3.16 and 3.17 is that NSP requires higher separation ratios for the same mobility when compared to the IPF. This is due to the auto-correcting feature of the IPF

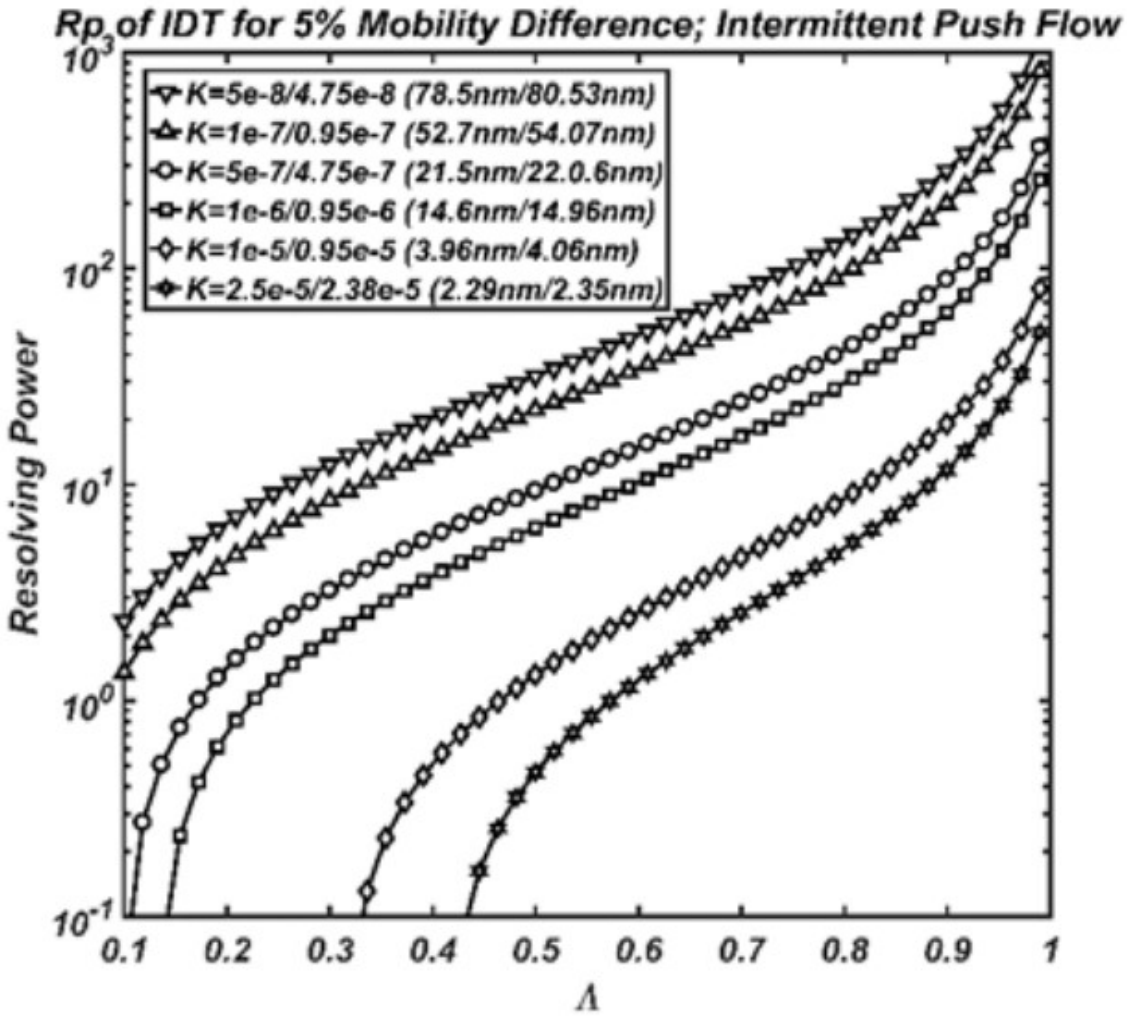

Figure 3.15. Resolving Power R_P as a function of separation ratio Λ ranges of ions with mobilities that differ 5% (2.23% in diameter) using Intermittent Push Flow

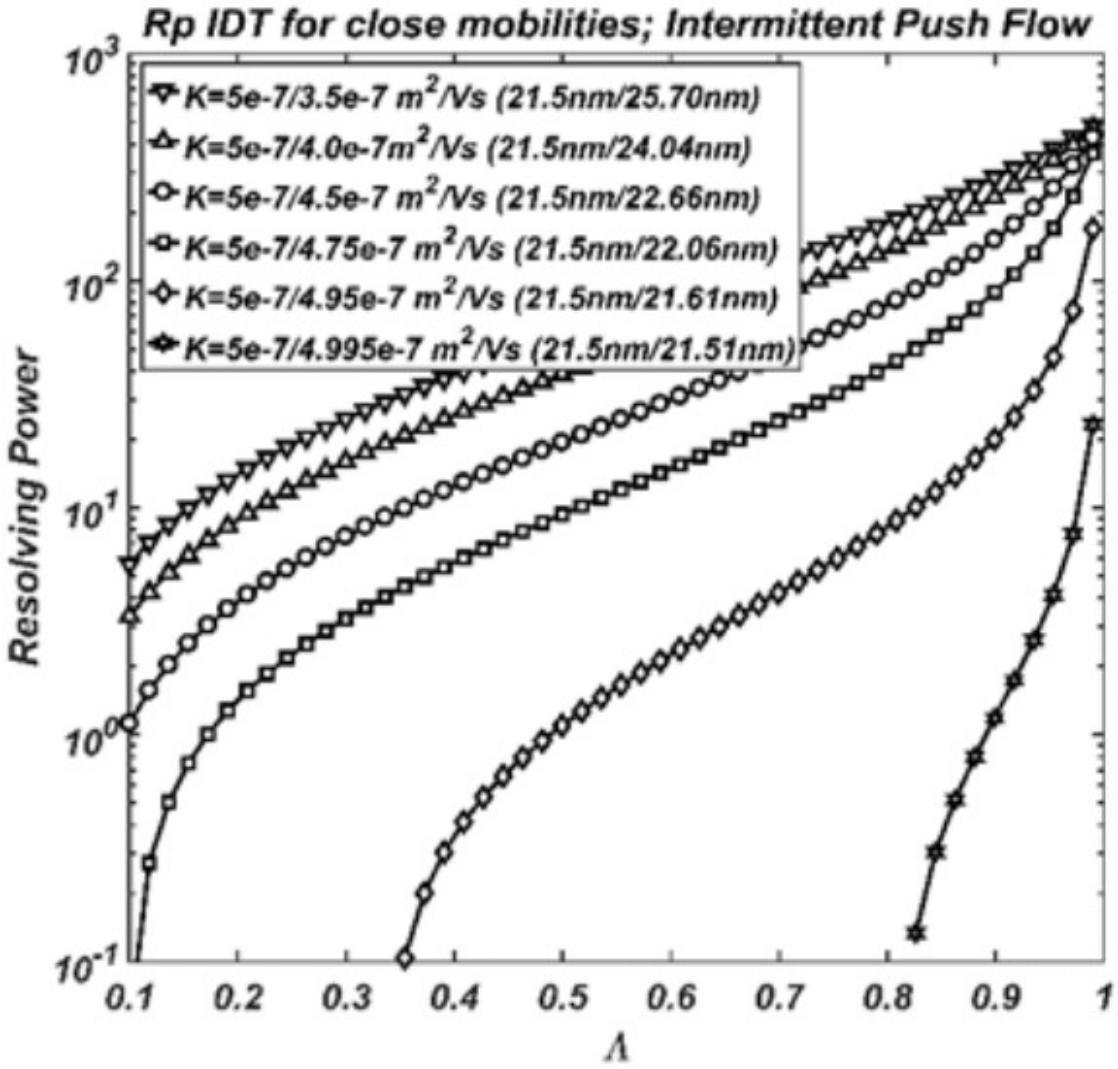

Figure 3.16. Resolving Power R_P as a function of separation ratio Λ for an Ion with Mobility of $5e^{-7}m^2/Vs(21.5nm)$ with respect to ions that differ between 30% and 0.1% in Mobility for Intermittent Push Flow.

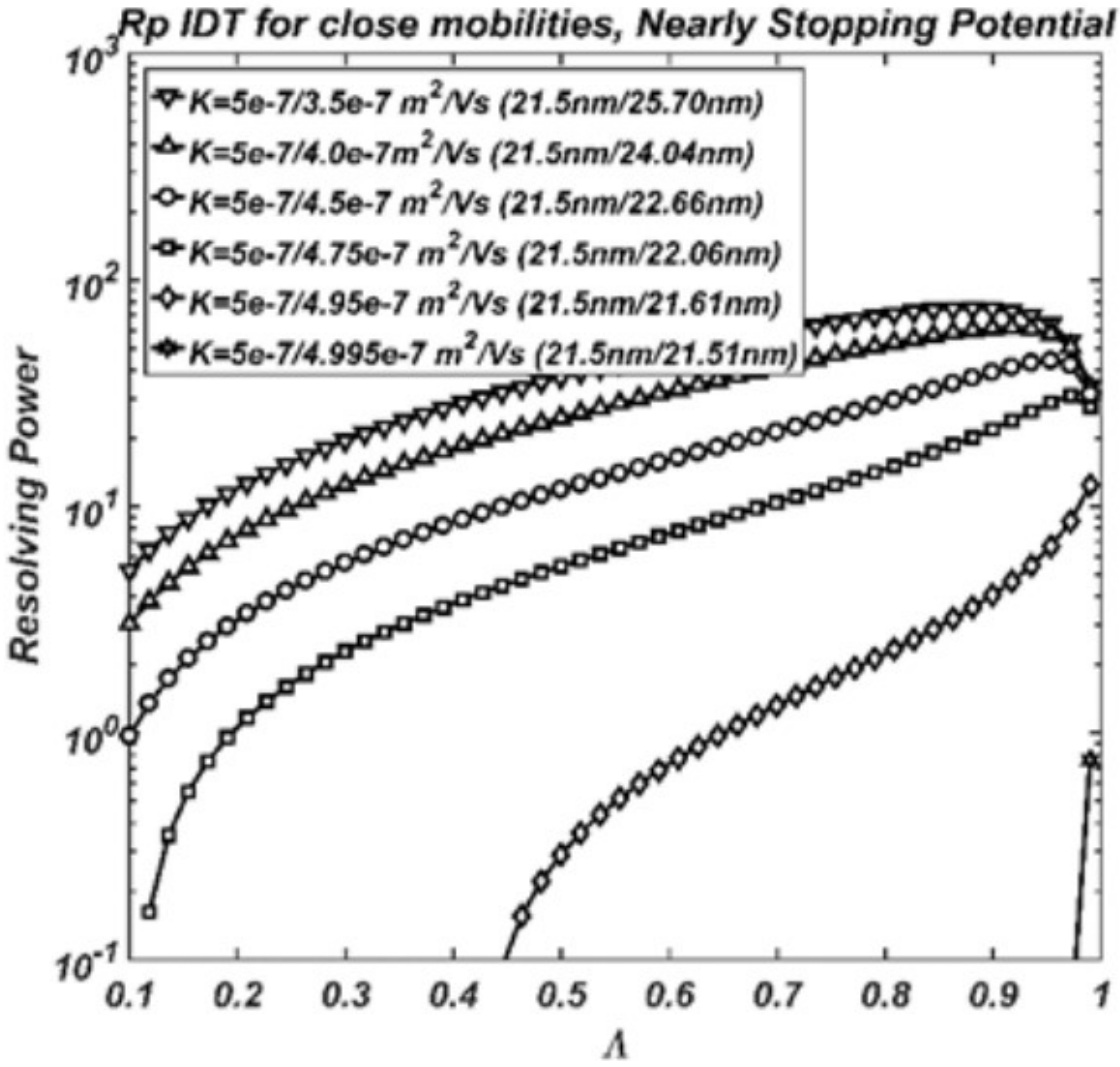

Figure 3.17. Resolving Power R_P as a function of separation ratio Λ for an Ion with Mobility of $5e\_{-7}m^2/Vs(21.5nm)$ with respect to ions that differ between 30% and 0.1% in Mobility for Nearly Stopping Potential.

disappearing when a constant electric field is used. This point can be made quite clear for low mobilities in figure 3.16. While, initially, increasing the separation ratio, Λ increases the Resolving Power, R_p, this increase reaches a maximum at around Λ=0.9 and then drops for larger values. At these very large residence times (large separation ratios), the diffusion velocity becomes of the same order or higher than the movement velocity v_m leading to a drop in R_p. However, the fact that the NSP can be used at higher separation ratios makes it a strong candidate for separation when compared to the IPF [28].

4. EXPERIMENT WITH IDT

4.1 Kanomax Drift Tube

For experimental purpose, Kanomax Inc. supplied one prototype of Drift tube which was better for testing purpose before making an actual prototype. However, the supplied drift tube varied from the designed model in different ways. The common comparisons in between our designed drift tube and kanomax drift tube are provided in table 4.1.

4.1.1 Formulations for Conducting Experiments

The position of a known mobility ion in the drift cell at any time t,

$$x_P = (v_{gas} - v_{drift})t \tag{4.1}$$

or,

$$x_P = v_{gas}(1 - \Lambda)t \tag{4.2}$$

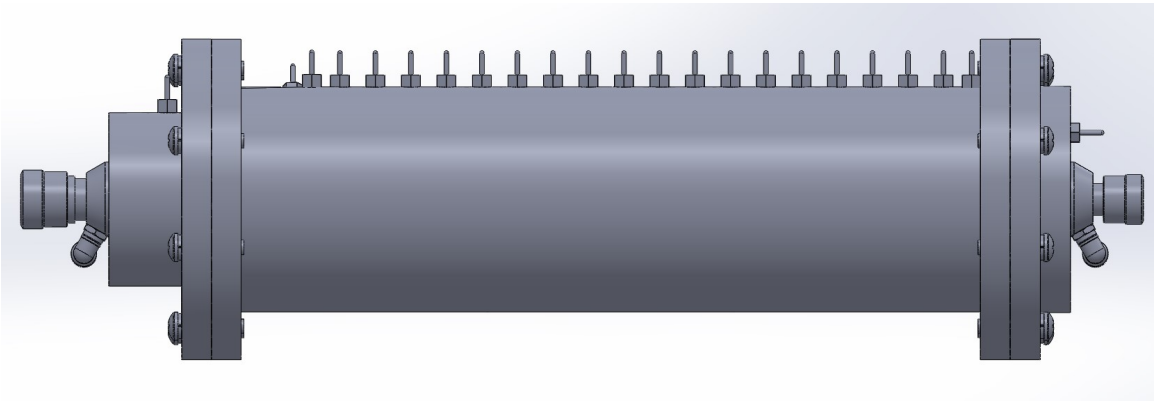

Figure 4.1. Kanomax Drift tube CAD model

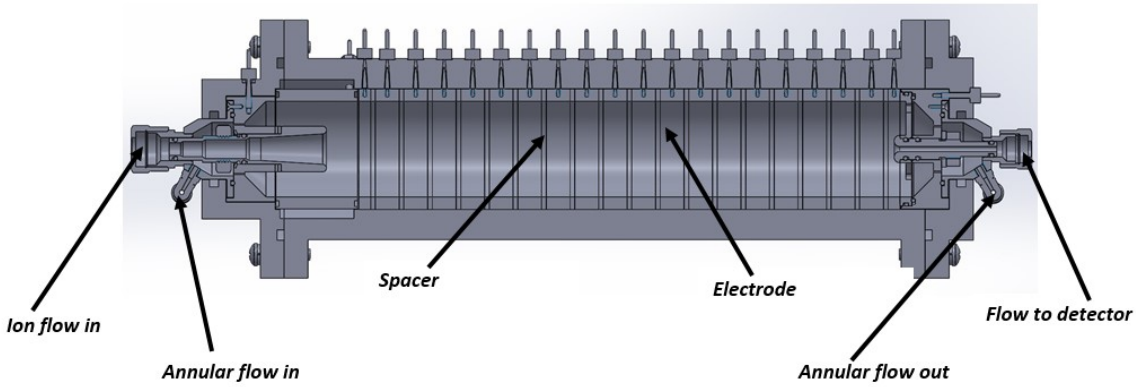

Figure 4.2. Kanomax Drift tube front sectional view

Table 4.1. Comparison in between designed drift tube and Kanomax drift tube

Comparison Types	**Designed Drift Tube**	**Kanomax Drift Tube**
Length	120mm	220mm
Inner diameter	48mm	45mm
Number of ring electrodes	30	20
Number of active electrodes	29 (1 was grounded)	16 (4 was grounded)
Width of spacer	2mm	10mm
Number of inlet and outlet	2 inlet and 1 outlet	2 inlet and 2 outlet

Where, Separation ration $\Lambda = v_{drift}/v_{gas}$. From the mobility equation (equation 1.1) we know,

$$v_{drift} = KE \tag{4.3}$$

Where K is the modified mobility at local temperature and pressure and E is electric field. The used equation of quadratic potential for IDT is,

$$V = Ax_p^2 \tag{4.4}$$

So the electric field becomes,

$$E = dV/dX = 2Ax_p = v_{drift}/K \tag{4.5}$$

or,

$$v_{gas} \times \Lambda/K = 2Ax_p \tag{4.6}$$

Replacing x_p in this equation from equation 4.1,

$$v_{gas} \times \Lambda/K = 2Av_{gas}(1-\Lambda)t \tag{4.7}$$

So, we can find the value of slope A from this equation,

$$A = (\Lambda/(1-\Lambda))/2Kt \tag{4.8}$$

The equation 4.8 represents slope A for the electric field as a function of time t and with time the slope A decreases if all the other parameters are kept constant. From equation 4.4, for full length L, using the value of slope A we get,

$$V = ((\Lambda/(1-\Lambda))/2Kt)L^2 \tag{4.9}$$

Also, the time needed t_{end} for a particular mobility particle to reach the length L is,

$$t_{end} = L/(v_{gas}(1-\Lambda)) \tag{4.10}$$

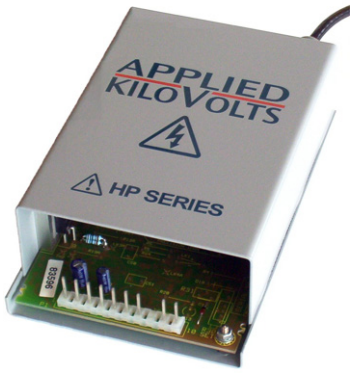

Figure 4.3. Applied Kilovolt HP005RAA025 series power supply

Figure 4.4. Emco (Model E121) power supply

4.1.2 Experiment Setup

Power Supply

Two power supplies were used in the experimental set up: One for providing the potential to the ring electrodes and another for providing high voltage for ion gating. A programmable Applied Kilovolt power supply was used for providing the potential to the ring electrodes which was controlled by a data acquisition system. The power output of this power supply could be instantly varied (within milliseconds) using control signal. The applied Kilovolt power supply could supply 0 to 5 KV based on the control signal 0 to 10V. The DAQ used (NI 6008) in experimental set up could only supply 5V analog signal, so, it was not possible to reach over 2.5KV using these power supply in the experiment.

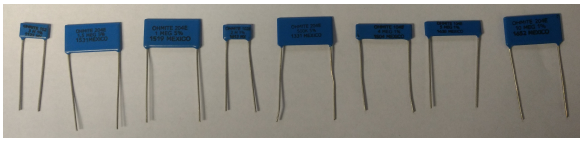

Figure 4.5. Resistors used for IDT

For providing high voltage to the ion gate an Emco type high voltage power supply was used. Using a pulsar a pulsed signal was provided to the Emco power supply. The higher and lower limit of the pulse was not varied with time.

DAQ

In the experiment, two NI 6008 DAQs were used for signal conditioning purpose. Both of the DAQs were connected to the computer and controlled by a LabVIEW software. One DAQ was used for providing pulse generator signal and at the same time for acquiring the analog input signal from electro-meter simultaneously. Another DAQ was used for providing control (analog output) single to the applied kilovolt power supply. The control signal was continuously varied from a set high voltage to low voltage based on the requirement of electric field ramping inside the drift tube. Figure 4.20 shows the NI 6008 DAQ.

Resistors

The supplied resistors with Kanomax Drift Tube were changed by a new set of resistors (ranging from 0.5 $M\Omega$ to 5 $M\Omega$). The used resistances are shown in figure 4.5. The new set of resistor was placed in between the ring electrodes for making the overall potential quadratic-electric field linearly increasing in the downstream direction. Table 4.2 shows the values of resistances in between two electrodes. The voltage and resistance configuration has been shown in Table 4.2 considering the highest voltage applied 2500V at one end.

Table 4.2. Potentials at different electrodes

Current (A)	3.22581×10^5	
No. of Electrodes	Resistances MΩ	Potential (V) in Different Electrodes
1	Grounded (0)	
2	Used for pulsing	
3	1	Grounded (0)
4	1.5	32.26
5	2	80.65
6	3	145.16
7	3.5	241.94
8	4	354.84
9	4.5	483.87
10	5	629.03
11	5.5	790.32
12	6.5	967.74
13	7	1177.42
14	7.5	1403.23
15	8	1645.16
16	9	1903.23
17	9.5	2193.55
18		2500.00
19		Grounded (0)
20		Grounded (0)

Figure 4.6. PVX-4130 ±6 KV pulse generator

Electro-Spray Ionization

As an ionization source, ESI was used in the experiment. For Ionization a separate high voltage arrangement was made (using the emco power supply). At the same time, one syringe was used to provide pressure for pushing the solution through the silica capillary. In the combination of pressure, the high voltage, as well as flow the electrospray, worked fine in the experiment to generate the electrospray. However, the ESI was very sensitive, and sometimes it was tough to make the Taylor cone. (see figure 1.3 for the Taylor Cone formation)

Pulser

One high voltage Pulsar was used to ion gate. As mentioned earlier, the DAQ could supply only 5V control signal, which was not enough for triggering the Pulse generator. So, using the DAQ as an external source at first a function generator was triggered, and then that function generator triggered the Pulse generator with 10 Vpp. From another side, one high voltage power source was connected to the pulse generator for providing high voltage pulsing. Figure 4.13 shows signal in and out for a pulsar.

Figure 4.7. Agilent 33521A 1-ch 250 MSa/s 30 MHz function generator

Ion Gating

One metal mesh was used for ion gating. The metal mesh was placed inside the drift tube and kept in touch with the no. 2 electrode. Then, the high voltage pulse was supplied from the pulsar to that electrode directly. The mesh being attached to the no. 2 electrode worked as ion gate. When the high positive voltage was supplied to the mesh no ion could penetrate inside the drift tube chamber. Ion could only penetrate inside the drift tube when the voltages went low. Another two meshes in both left and right of the gate mesh were placed and grounded. They were placed to make a barrier to the high electric field created by the pulsar voltage so that the ions were not affected by the pulsar voltage.

Flow Meter

As mentioned earlier the Kanomax Drift Tube had two inlets: One inlet was in the middle of the drift tube, and another inlet was through the side, it is better to demonstrate this as annular flow. Following inlets, it had two outlets: One was in the middle and directly connected to the electro-meter sensor, and another one was the side outlet or annular outlet (see figure 4.2). Four flow meters were used for controlling flow rates in these four inlets and outlets. The middle inlet flow which also contained positive ions was controlled by one rota-meter, and the side flow was controlled by one TSI flow meter. At the outlet side, The flow to the detector was controlled by TSI flow meter, and the annular outlet flow was controlled by another rota-meter. Both of the rota-meters were calibrated by the TSI flow meter. Figure 4.14 demonstrates the inlet and outlet flow as well as the flow meter positions.

Figure 4.8. TSI 4100 series flow meter (max flow capacity 20 L/min)

Figure 4.9. Cole parmer rota-meter (maximum flow capacity 15 L/min)

Figure 4.10. Swagelok stainless steel integral bonnet needle valve, 0.37 Cv, 1/4 in.

Flow Control Valve

Three Stainless Steel Integral Bonnet Needle Valve were used in the experiment: one for controlling the annular flow inlet and other two of the two outlets. The flow control valve was essential to control the flow rate inside IDT.

Pump

A 1/6 HP piston air vacuum pump was used in the experimental set-up. The pump was directly connected to the outlet via the flow meter and flow regulator. The pump was used to suck air from the drift tube, making the flow of gas from the upstream to downstream direction. Figure 4.14 shows the position of pump in the experimental setup.

Electro-meter

For detecting the ions in experiment one electro-meter was used. The electro-meter was connected with one Analog to Digital converter (ADC), and the signal was transferred to the computer using NI 6008 DAQ analog input channel. The signals were recorded in the LabVIEW software. From the LabVIEW software, the data were collected and saved for further analysis.

Figure 4.11. 1/6 HP piston air compressor/vacuum pump, 115VAC, 50/50 Max. PSI Cont./Int.

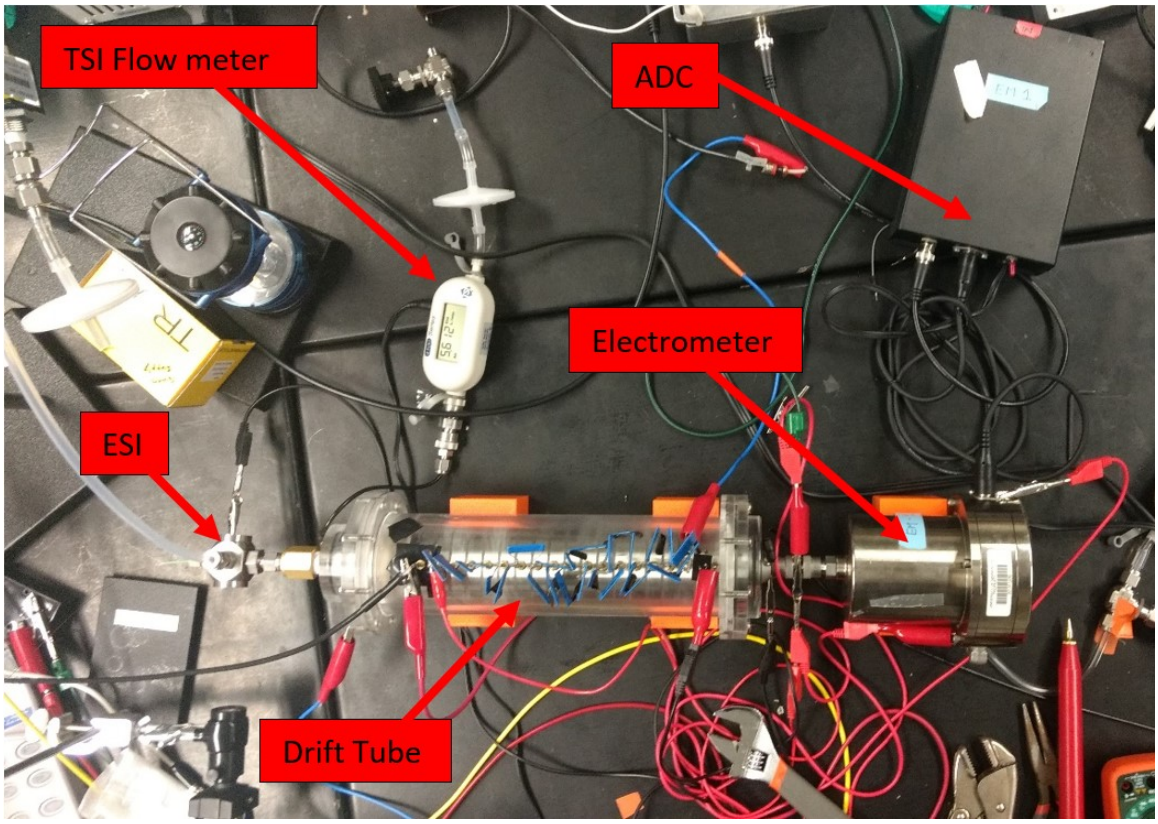

Figure 4.12. Electro-meter and ADC

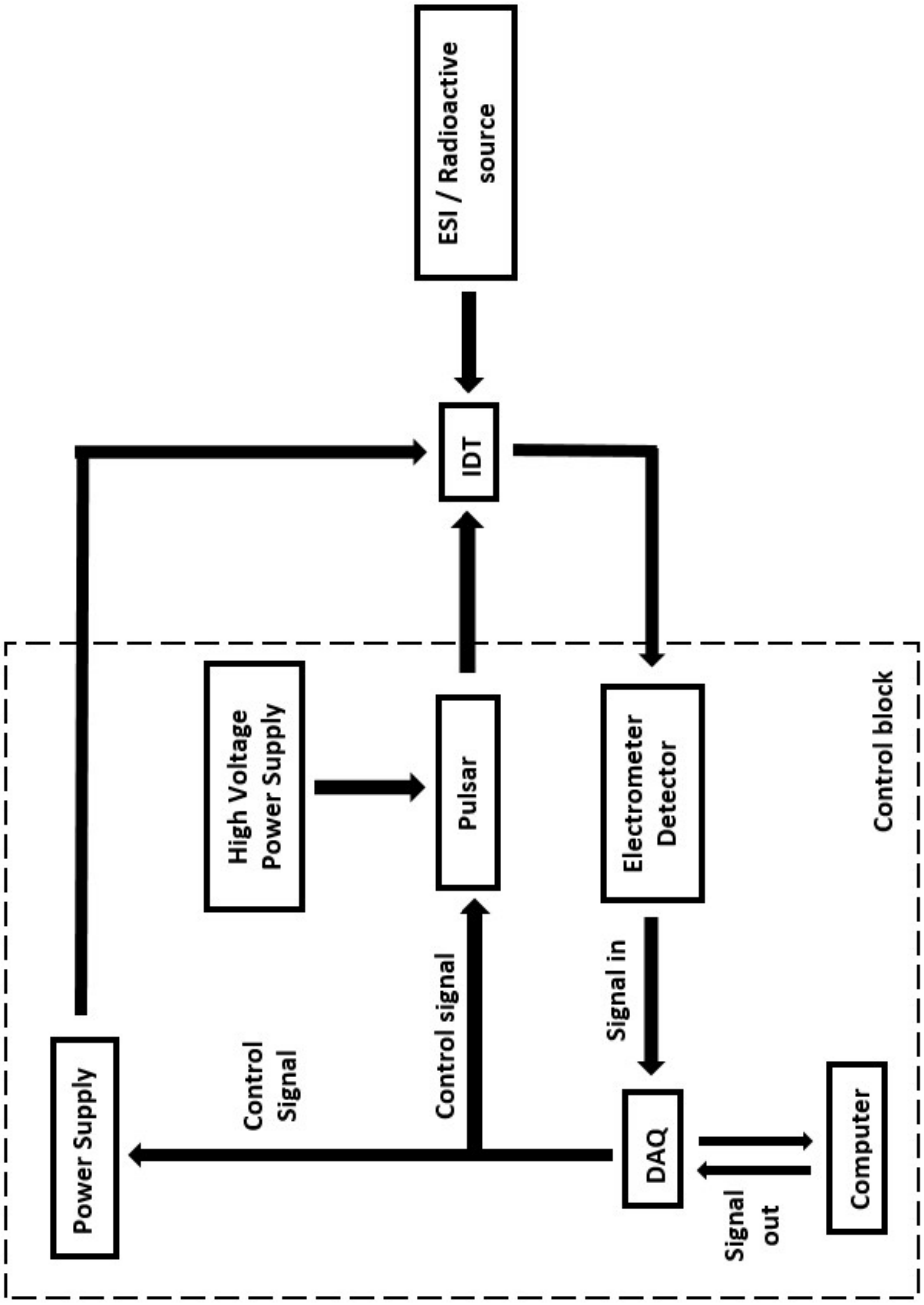

Figure 4.13. Flow Chart of IDT working system

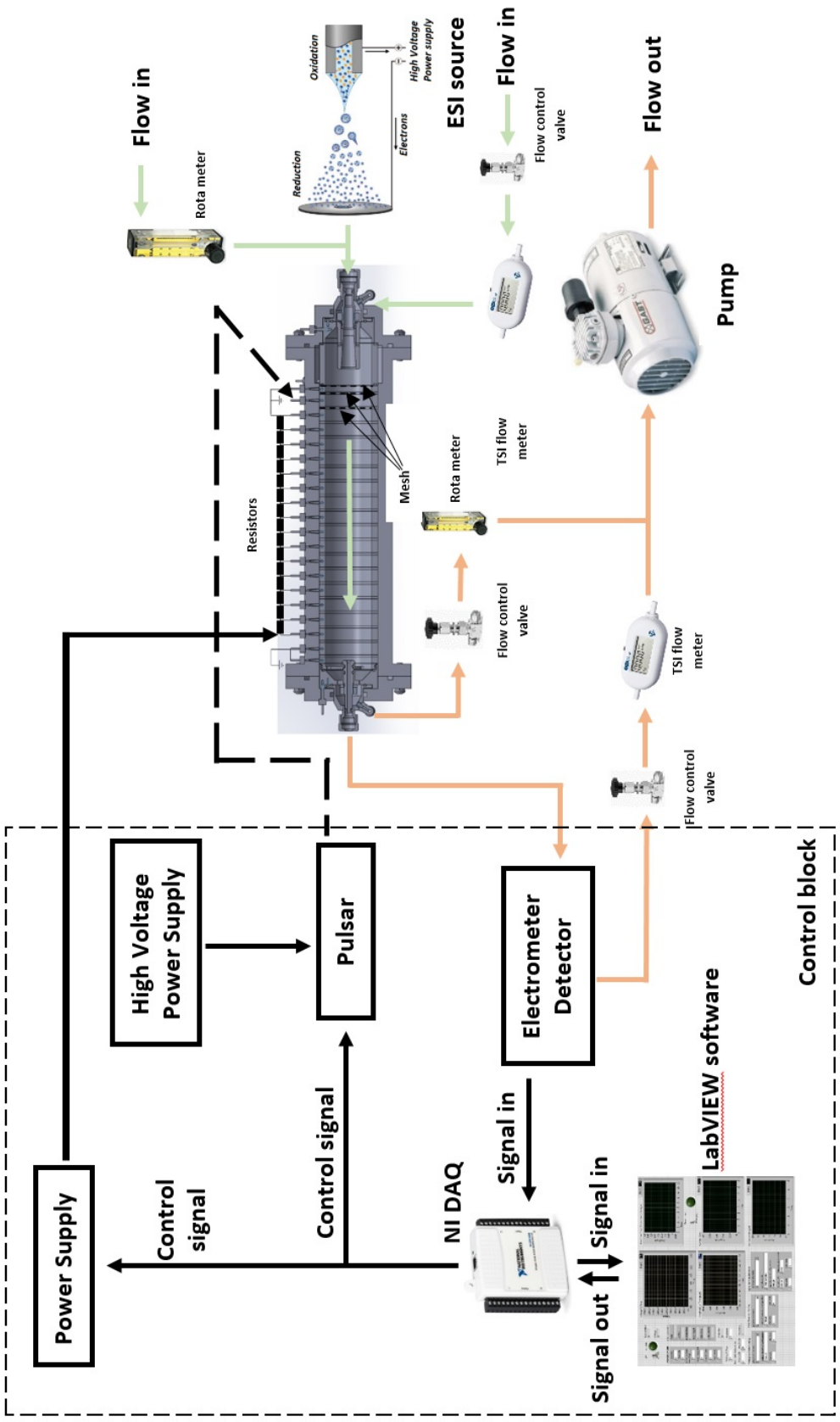

Figure 4.14. Experimental set up flow chart

LabView Software

A Lab View software was made for conducting the signals to DAQ and at the same time for collecting the signal from DAQ.

The total LabVIEW program can be divided into four parts, and they are: 1) input parameters, 2) calculated parameters 3) signal in and 4) signal out.

Input Parameters

The Lab View program considers the following Input parameters:

1. Diameter of ions
2. Separation ratio
3. Local Pressure
4. Local Temperature
5. Length of DT
6. Velocity of gas

Calculated Parameters

1. Mass of ion: The masses of the ions were calculated from the following formula (source: atmospheric aerosols 14-35 Handbook of Chemistry and Physics 83rd edition):

$$mass_{ion} = (d_{ion}/0.120415405)^3 \tag{4.11}$$

2. Mobility: The mobility K_0in air for selected ion was calculated from the following equation (source: atmospheric aerosols 14-35 Handbook of Chemistry and Physics 83rd edition):

$$K_0(10^{-4}m^2V^{-1}s^{-1}) = 1 \times 10^{-5} \times 10^a \tag{4.12}$$

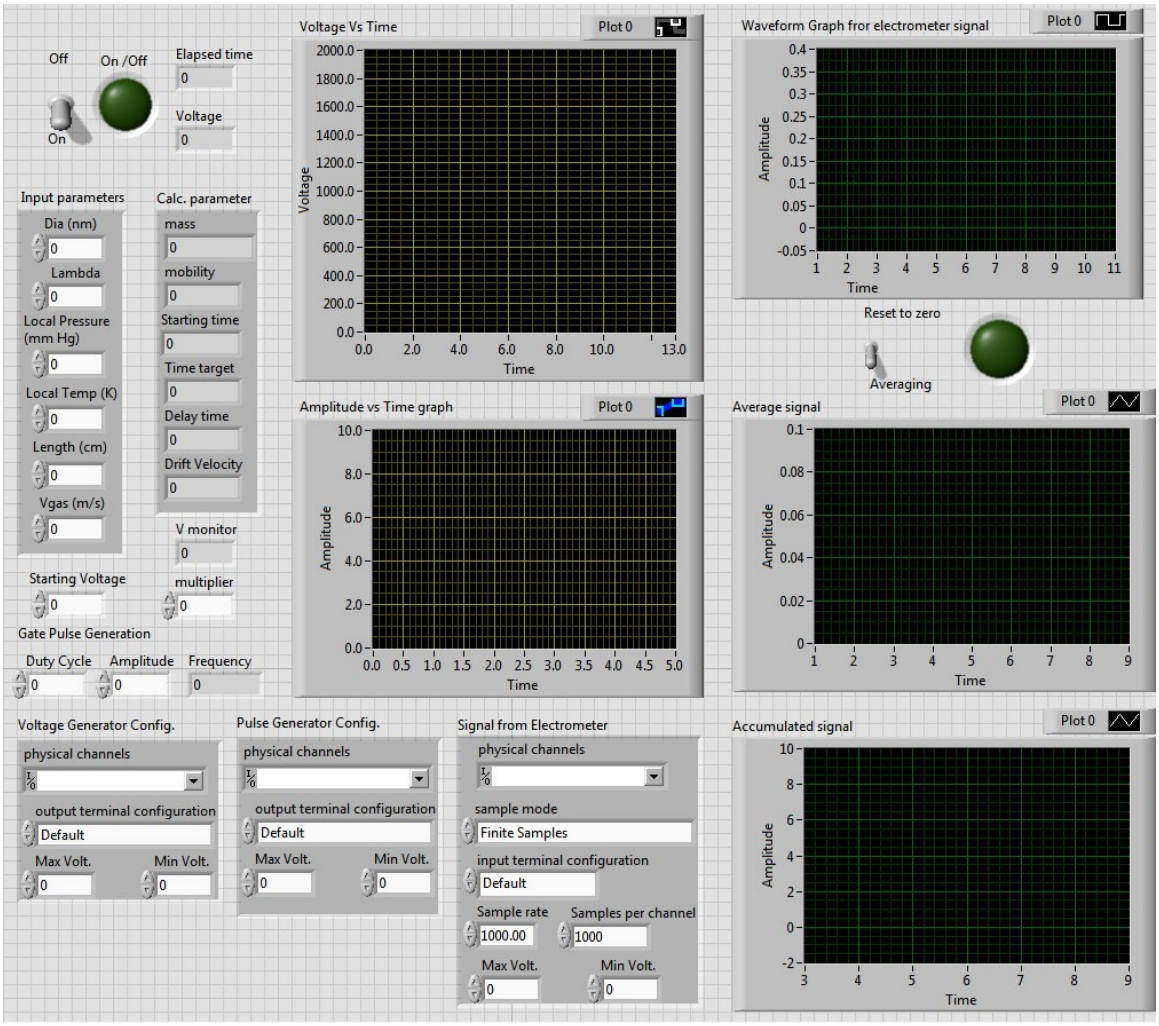

Figure 4.15. GUI of IDT software made in LabVIEW

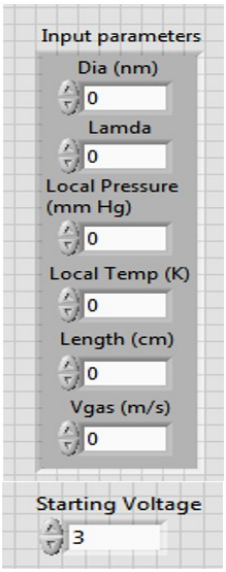

Figure 4.16. Input parameters in Software

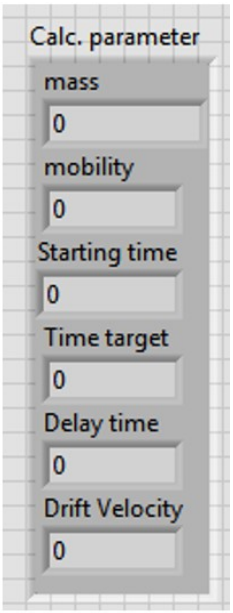

Figure 4.17. Calculated parameters in Software

Where,

$$a = 4.9137 - 1.4491\log(d(nm)) - 0.2772(\log(d(nm)))^2 + 0.0717(\log(d(nm)))^3 \tag{4.13}$$

Based on the local pressure P and temperature T the the modified mobility K was calculated as,

$$K = K_0 \times (760/P) \times (T/273.15) \tag{4.14}$$

3. Starting time: Starting time was always set zero by default.

4. Time Target: The time target was found using the formula 4.10.

5. Delay Time: From equation 4.9 the voltage corresponding the starting time $t = 0$ was very high which may cause harm the Drift tube as well as any electrical equipment attached to that Drift tube. So, a time delay was set based on the maximum attainable starting voltage. During the time delay, the applied voltage was kept constant to the set maximum starting voltage. After that time delay, the voltage varied with time. The limitation of maximum voltage supply

was $2.5kV$ (as mentioned in Pulsar section). Delay time was calculate from equation 4.9 by the little rearrangement:

$$t_{delay} = 2VK/(\Lambda(1-\Lambda)v_{gas}^2) \tag{4.15}$$

6. Potential: The variation of potential with time was set using equation 4.9.

7. Drift velocity: Drift velocity $v_{drfit}$was calculated for a given gas velocity v_{gas} as follow:

$$v_{drift} = \Lambda \times v_{gas} \tag{4.16}$$

where, Λ was separation ratio.

Signal In and Out

Two different NI6008 DAQ were used for signal in and out. From one DAQ an analog signal for pulse (0-5V) was supplied for the calculated target time, t_{end}. It was controlled by the Duty cycle and amplitude. The same DAQ was used for getting the signal from the electrometer. The sample rate and sample per channel, sample mode and sample input terminal all were configured before running the software. From another DAQ, an analog control signal was supplied to the power supply to provide electric field inside the drift tube which varied with time.

4.1.3 Results from Experiment and Validation

Experiment with Constant Voltage

In the experiment, the solution used was 20% 1 mL Ionic Liquid (1-Ethyl-3 methylimidazolium tetrafluoroborate). The 1mL solution was prepared in a vial by mixing 200 μL Ionic liquid with 400 μL water and 400 μL methanol. Using the ESI arrangement (see section Electro Spray Ionization) this solution was sprayed inside the IDT.

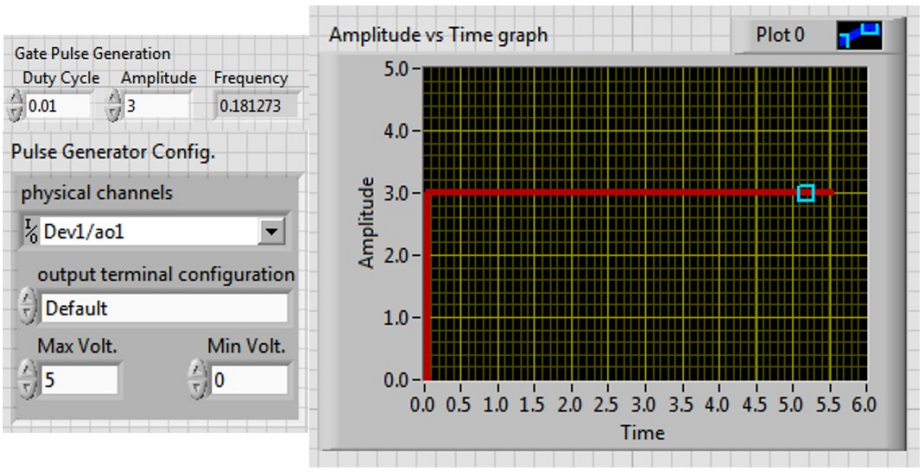

Figure 4.18. Pulse generator signal from NI 6008 DAQ

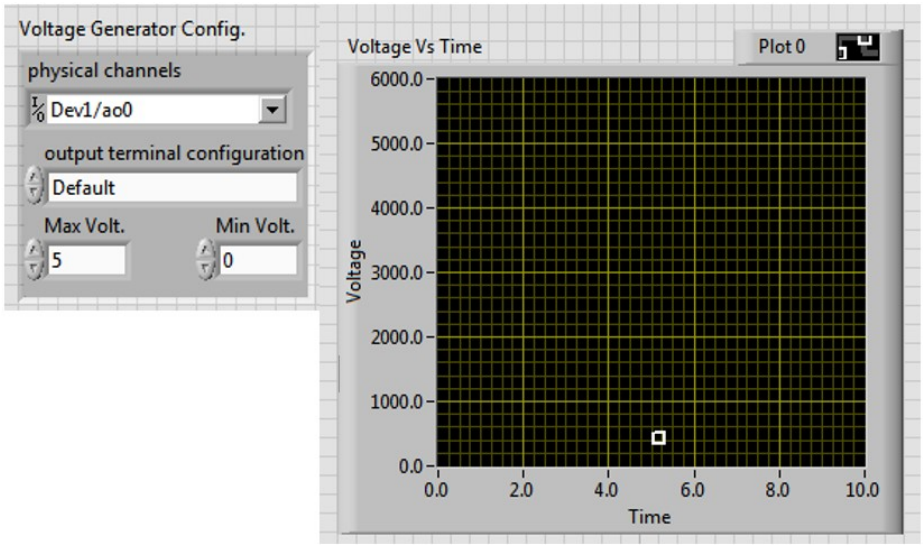

Figure 4.19. Voltage generator signal from NI 6008 DAQ

Figure 4.20. NI 6008 data acquisition tool used for both signal and In and Out

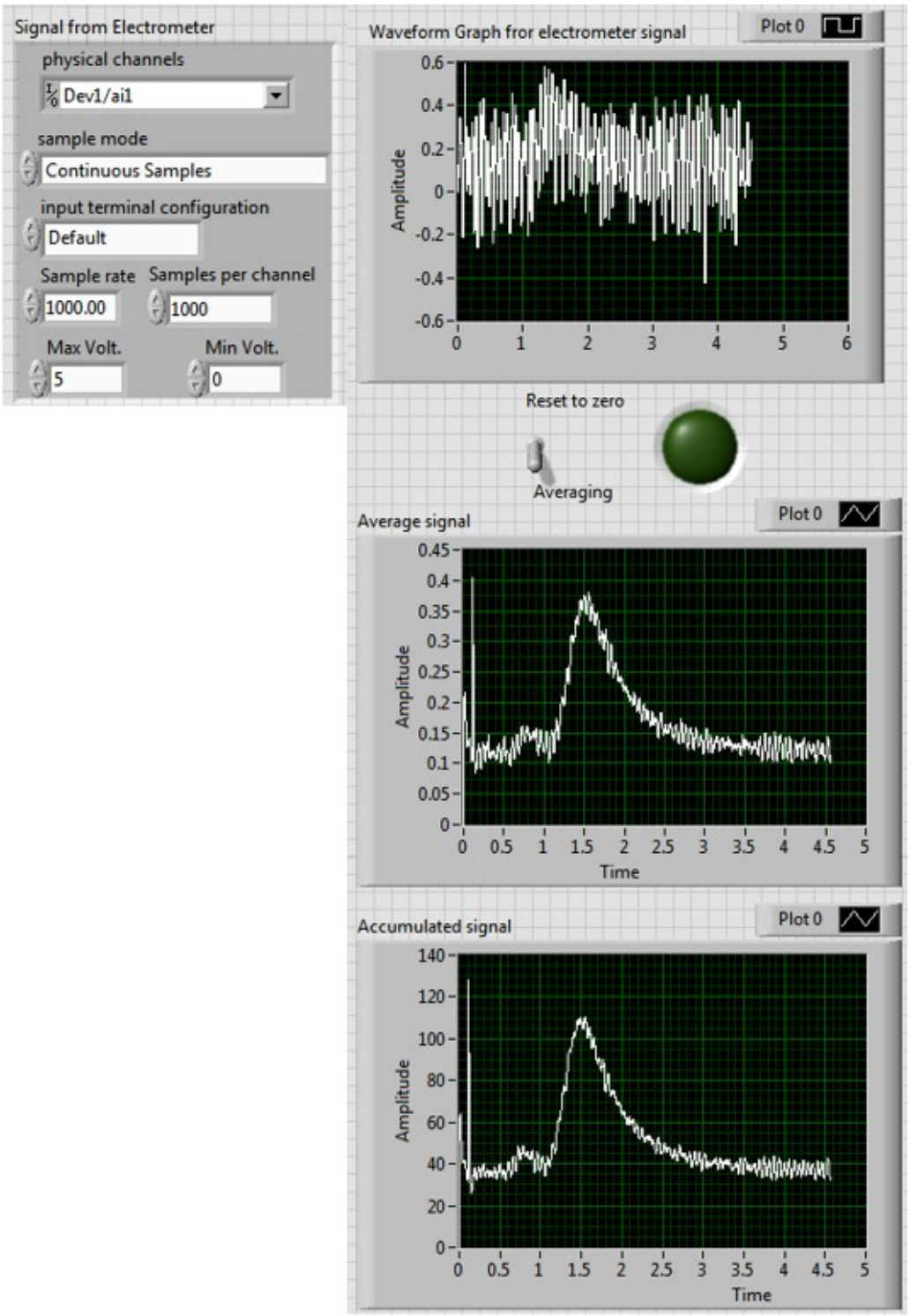

Figure 4.21. Generated signal in IDT software

In the first trials, the supplied voltage was varied from 300V to 750V with a step of 50V. With increasing the voltage (350V to 600V), the peak broadening occurred due to separation, however, it could not resolve two separate peaks at that low voltage range. In high voltage, starting from 650V, the instrument started resolving double peaks. Flow rates at the two inlets and outlets were controlled by the flow meters. The total flow rate measured from the flow meter was 13.6 L/min. The velocity inside the tube was found around 12 m/s - flow rate divided by the cross-section of the drift tube. However, that was not correct as the flow pattern inside the tube was completely unknown and complicated to find. To find the actual velocity of the particle a different tactic was used.

As the biggest particles moved with the velocity of the gas (due to inadequate electric field to stop them) and were the first group to be detected, so, the actual flow velocity inside the tube can be found by dividing the total distance (length of tube) by the instantaneous signal starting point (starting time of peak). It was mentioned earlier that the active number of electrodes used in the experiment were 16 of 10 mm each and 2 mm spacers were in between two electrodes. Considering the widths of the ring electrode and the spacers, the total length of travel distance was calculated 190 mm. The extra length at the inlet and outlet side were neglected as the cross-sectional areas at the inlet and outlet section were minimum (1/4 inch diameter). So, it was expected that the particles would pass those lengths within the fraction of milliseconds. As a result, that length would not affect the time count very badly. The signal starting point was 0.7 s, and considering the length 0.19 m, the calculated velocity inside the drift tube was 0.225 m/s.

Figure 4.22 shows the raw orange signal (peak) represented the distribution of ions when no voltage was applied. For no applied voltage, there was no separation, and the width of the peak was 0.3 s only (time at signal ending point - time at signal starting point). For constant high voltage, 750 V, however, the two peaks were resolved (blue color), and the width of distribution became more than 2.3 s which represented a very good separation of ions.

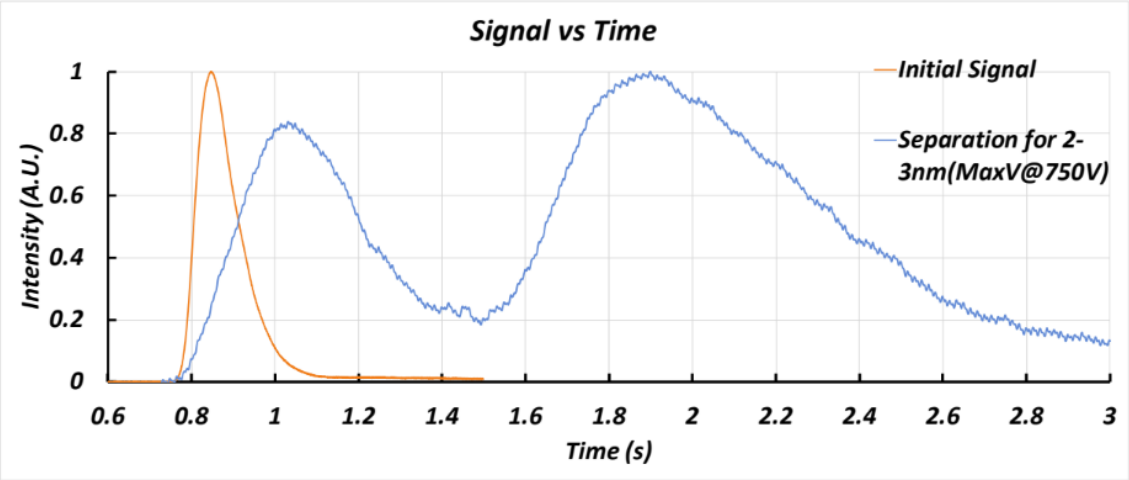

Figure 4.22. Raw data (averaged over time) of the separation for 5nm using a maximum voltage of 750V.

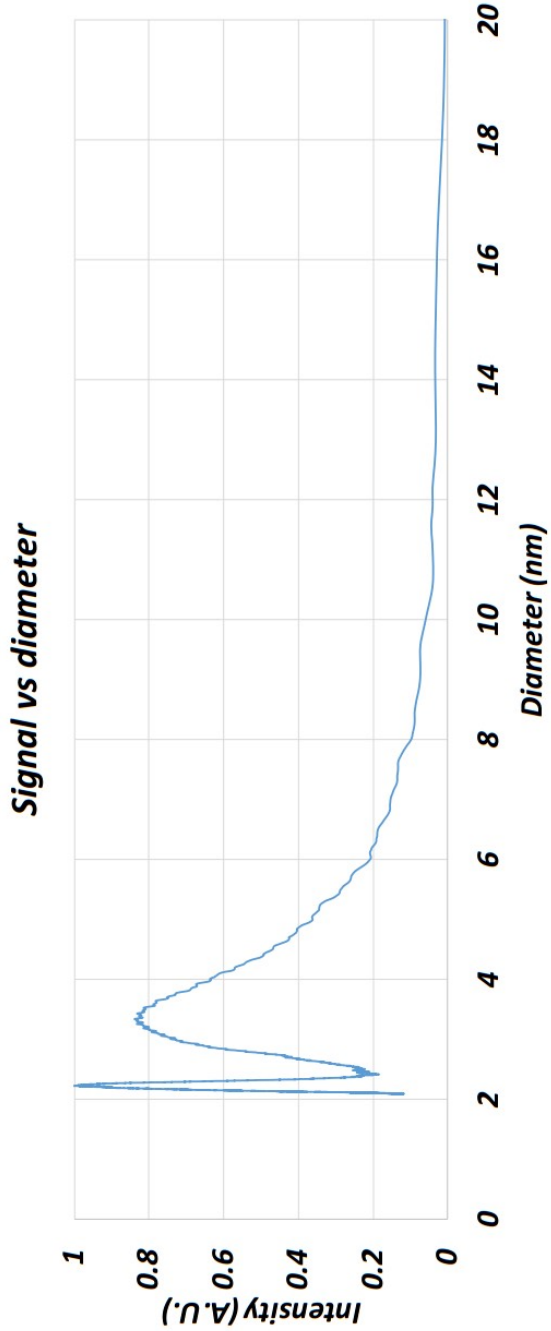

Figure 4.23. Time transformed into diameter

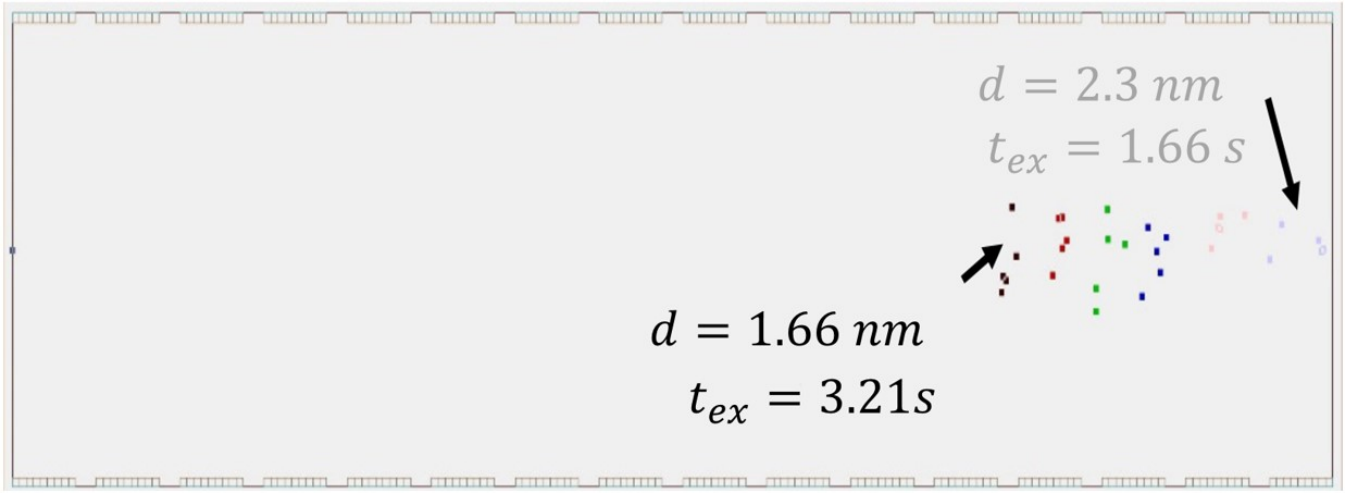

Figure 4.24. Particle separation in SIMION for constant applied voltage, 750 V

Conversion of Time to Mobility

According to the equation 4.9, at time t=0 the voltage would be infinitely high which was impossible to achieve. So, in software, there was one option called initial voltage or maximum voltage V_{max}. The initial voltage was kept fixed for a particular time, t_{delay}. This t_{delay} was the time when the decreasing voltage (from equation 4.9) is just below the initial voltage V_{max} (see the section Delay Time). Another assumption can be made, during t_{delay} time the particles reached x_{delay} distance. The equation of particles of a given mobility to reach distance L at time t would be:

$$L = (x_{delay} - (1-\Lambda)t_{delay}v_{gas})(t/t_{delay})^{-(\Lambda/(1-\Lambda))} + (1-\Lambda)v_{gas}t \tag{4.17}$$

where

$$x_{delay} = v_{gas}/2KA(1 - e^{-2KAt_{delay}}) \tag{4.18}$$

and

$$t_{delay} = \Lambda_0/(1-\Lambda_0)L^2/2K_0V_{max} \tag{4.19}$$

Equation 4.18 can be solved for mobility as a function of time using Lambert W function. As the mobility was also a function of diameter, so, in the end, the time was completely transformed to the diameter of the particle. A similar transformation was done for the signal showed in figure 4.22, and the transformed signal is showed in figure 4.23 which represented that the system separated the 1.66 2.3 nm diameter ions within complete 1 second of the time difference.

For validating the experiment result with the simulated result, a SIMION model of the kanomax Drift Tube was prepared only taking into account the 16 electrodes each of 100 mm width and 15 spaces of 2 mm width to mimic the actual Kanomax Drift Tube. The potentials applied to the electrodes were of quadratic order (increasing with distance), and the highest voltage was set to 750V. Collision SDS model also applied in the SIMION program, and the X directional velocity, V_x was considered 0.225 m/s. The particle, selected to fly through the drift tube, were given in table 4.3. To observe the separation of 1.66 to 2.3 nm particles more closely, only the charged particles of that range were selected.

Table 4.3. Particles selected for validation

Mass (amu)	Diameter (nm)	Mobility ($m^{-2}V^{-1}s^{-1}$)
2619	1.66	4.09e-5
5000	2.06	2.91e-5
5500	2.13	2.77e-5
6000	2.19	2.64e-5
6500	2.25	2.53e-5
7000	2.30	2.43e-5

From simulation, the same complete separation of 2 3 nm particles within 1 s time period were found, which obviously validates the instrument for constant voltage separation.

Experiment with Variable Voltage

For testing the instrument with variable voltage (continuous ramping of the electric field), the maximum voltage applied to the instrument was 2000 V corresponding to control signal of 4V from DAQ. The ion inlet flow rate was 4.03 L/min, and the annular flow was set to 4.73 L/min. For this experiment, only one outlet was used to capture most of the ions based on the assumption that some ions might leak through the annular flow. The total flow at the outlet was 9.03 L/min. The separation ratio Λ used in the software was 0.5. For Different diameter, the signals were found. Figure 4.25 represents the progression of the signal for set diameter 1 nm diameter to 4 nm diameter in the software.

SIMION Simulation for Varying Voltage

Figure 4.25 shows, at no voltage (zero voltage) condition, the peak was thinner, and with increasing the voltage (going towards the higher value of diameter in software), the peak became wide which again represents the higher separation with higher applied voltage. From 1.8 nm diameter to higher diameter the peak became much wider, and two peaks were resolved though, they were not completely separated. From figure 4.25 the initial peak width (with zero voltage) 0.4 s which changed to 2.4 s for the voltage set for 4 nm diameter.

The .Lua program in SIMION was changed for implementing this variable voltage with time. In SIMION for declaring the quadratic potential instead of using 4.4, the following formula was used,

$$V = A(n_P - 1)^2 \tag{4.20}$$

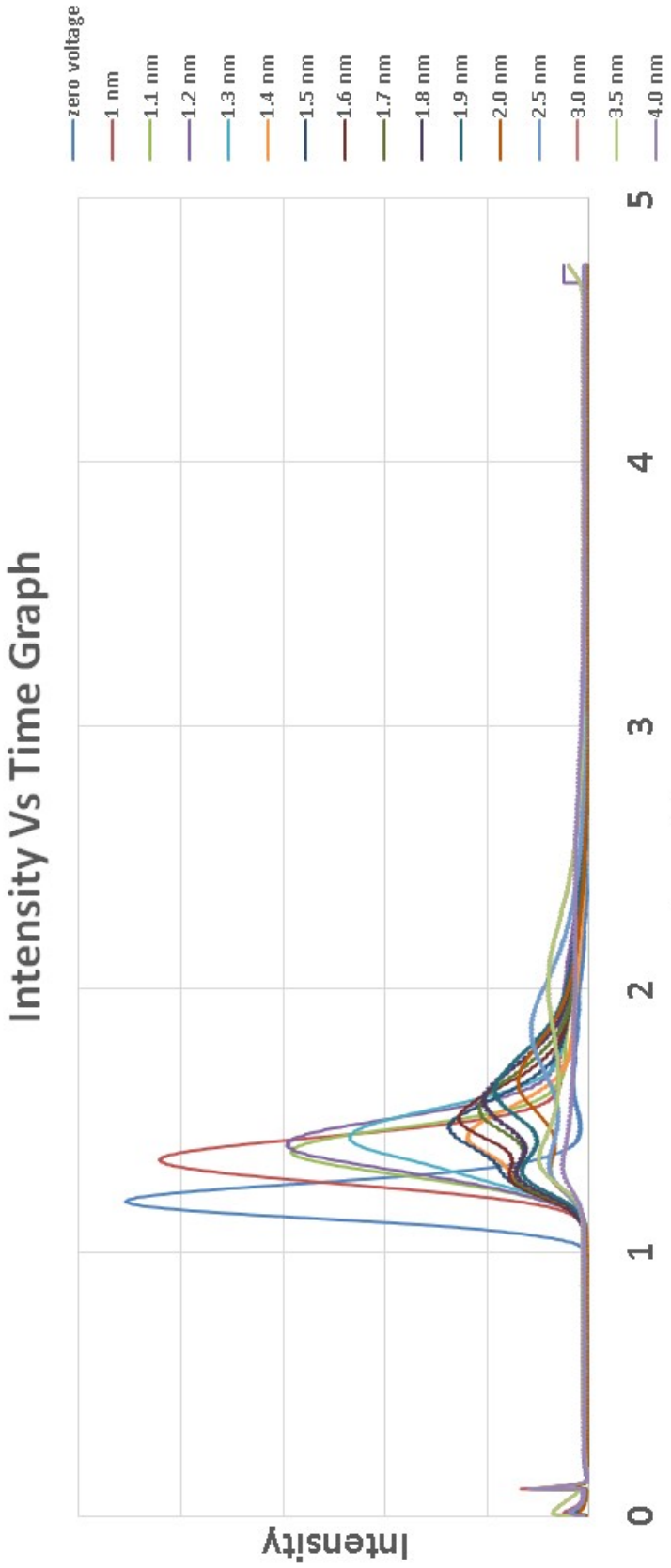

Figure 4.25. Progression of signal from 1 nm to 4 nm set diameter

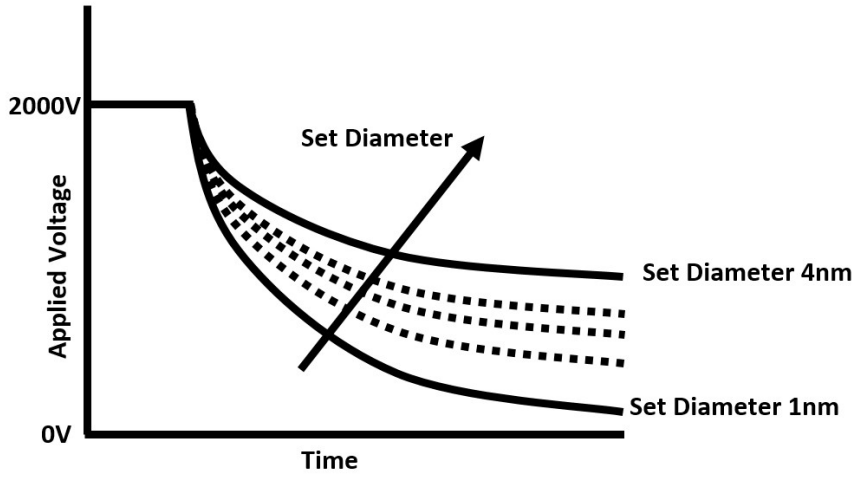

Figure 4.26. Change of supply voltage with time for different diameters

Where, n_P is the number of electrodes. We had total 16 electrodes for Kanomax Drift tube, So $n_p = 16$.

The maximum voltage V_{max} was found from equation 4.9 for different time t.

The slope was found as.

$$A = V_{max}/15^2 \tag{4.21}$$

As, $(n_P - 1) = 15$ and this slope A was then used in equation 4.17 to find the potentials at different electrodes by changing n_P from 1 to 16.

The change of voltage corresponding to different diameter is shown in figure 4.26. The starting voltage was 2000 and the constant horizontal line before the voltage decrement represents time delay. Figure 4.26 also shows that with increasing the set diameter the voltage decrement shifts to the higher side, which represents more separation in another sense.

The voltage in SIMION also varied as shown in the figure 4.26. Two simulation works were performed in SIMION with the input parameters shown in table 4.4, and the selected particles are shown in table 4.5. The axial velocity v_x was assumed 0.173 m/s as calculated from the actual experiment.

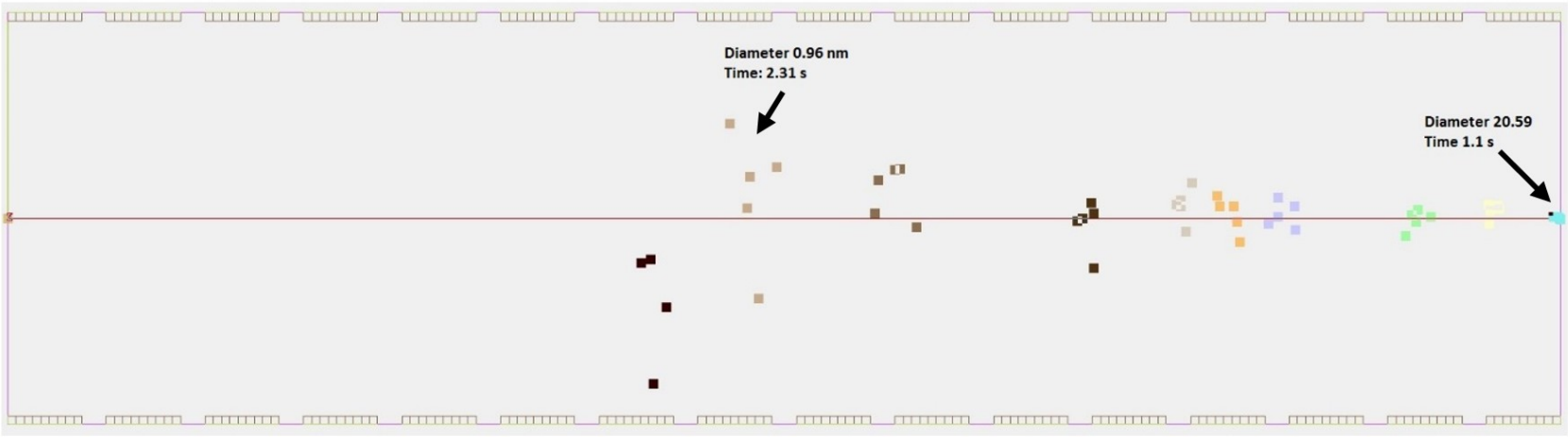

Figure 4.27. SIMION simulation of different diameter 0.81 to 20.59 nm diameter particles for set diameter 1 nm in software

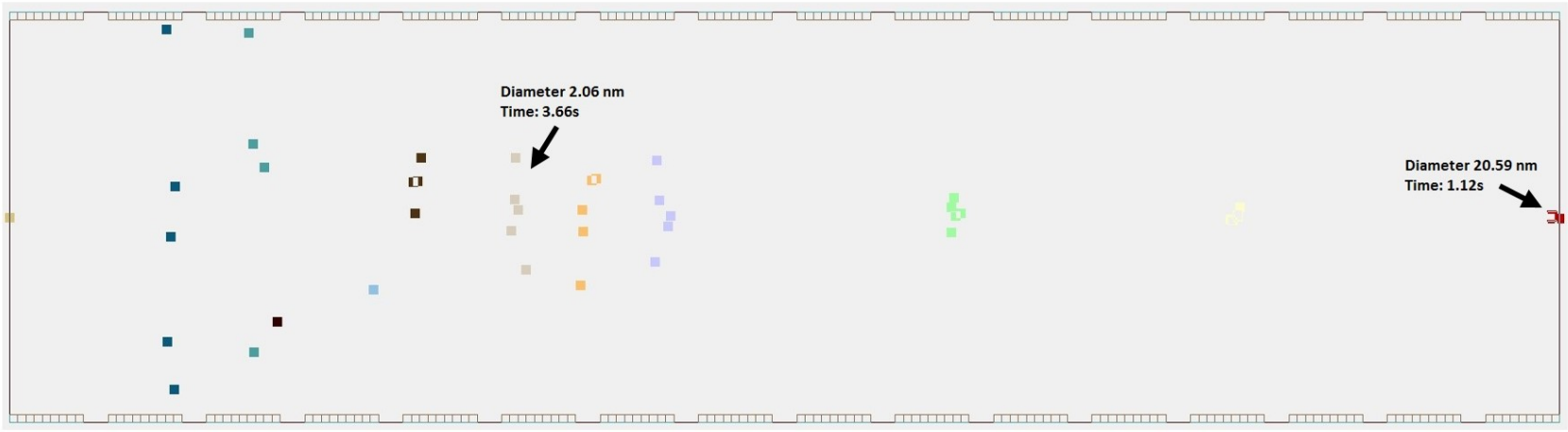

Figure 4.28. SIMION simulation of different diameter 0.81 to 20.59 nm diameter particles for set diameter 4 nm in software

Table 4.4. The input parameters in SIMION

	Simulation 1	Simulation 2
Length of IDT	0.19m	0.19m
Λ	0.5	0.5
Set Diameter	1 nm	2 nm
Set Mobility	8.79359E-05 $m^2V^{-1}s^{-1}$	9.70264E-06 $m^2V^{-1}s^{-1}$

Table 4.5. Particle selected for SIMION simulation

Mass (amu)	Diameter (nm)	Mobility ($m^2V^{-1}s^{-1}$)
300	0.806100398	1.19E-04
500	0.955737703	9.39E-05
1000	1.20415405	6.69E-05
3000	1.736690661	3.82E-05
5000	2.059074462	2.91E-05
7000	2.303463831	2.43E-05
10000	2.594271257	2.00E-05
30000	3.741586606	1.09E-05
100000	5.589187992	5.45E-06
5000000	20.59074462	5.31E-07

From figure 4.27, SIMION showed the biggest particle of 20.59 nm reached the detector at 1.1 s for both the 1 nm diameter, and 4 nm diameter set conditions, meaning the system could not at all separate the 20.59 nm particles. However, in case of lower side voltage decrement (set diameter 1 nm), the separation was not good for the biggest particle as expected and separation was good for 0.96 to 3.74 nm particles, which was exactly in agreement with the signal showed in table 4.25 for 1 nm diameter particles. On the other hand, for high side voltage decrement (set diameter 4 nm), the separation shifted from lower diameter particles to higher diameter particles. SIMION showed good separation (see figure 4.28) for 3.74 to 2.06 nm particles for 4 nm set diameter condition and the time span was also in agreement with the signal showed in figure 4.25 for 4nm set diameter. In all conditions, the simulations provided very good representations of particle separation according to actual concept.

5. SUMMARY

5.0.1 Conclusion

A new mobility particle analyzer, which has been termed Inverted Drift Tube, has been modeled analytically as well as numerically and proven to be a very capable instrument. The basis for the new design have been the shortcomings of the previous ion mobility spectrometers, in particular, a) diffusional broadening which leads to degradation of instrument resolution and b) inadequate low and fixed resolution (not mobility dependent) for large sizes. To overcome the diffusional broadening and have a mobility based resolution, the IDT uses two varying controllable opposite forces, a flow of gas with velocity v_{gas}, and a linearly increasing electric field E that opposes the movement. A new parameter, the separation ration $\Lambda = v_{drift}/v_{gas}$, is employed to determine the best possible separation for a given set of nonparticipants [28]. Due to the systems need to operate at room pressure, two methods of capturing the ions at the end of the drift tube have been developed, Intermittent Push Flow for a large range of mobilities, and Nearly-Stopping Potential Separation, with very high separation but limited only to a very narrow mobility range. The following conclusions have been obtained:

- Analytical description of the 1D IDT problem for an initial distribution of nonparticipants has been shown to yield very high resolutions without any optimization. Resolution is close to being proportional to the square root of the length but has a dampening effect on the standard deviation that increases the resolution several folds when compared to a drift tube. The resolution is also proportional to the mobility. The lower the mobility, the higher the resolution. However, it is shown that the resolution is an ill-conditioned parameter to express whether or not separation occurs inside the drift cell.

- A 1D numerical simulation of the IDT shows that there is an asymptotic value to the standard deviation for the intermittent push flow method. Regardless of the starting distribution, whether broad or narrow, the asymptotic behavior is achieved. The IDT has auto-correcting capabilities and fixes the diffusional broadening existing in other commercial instruments.

- 3D numerical simulations for single particle trajectories using stochastic diffusion in SIMION for the IDT are used to obtain resolutions of ions and separation ratios. Intermittent Push Flow resolutions acquired agree qualitatively with those predicted analytically. For Nearly-Stopping Potential Separation, the modeling of the instrument is shown to be able to separate particles of 55.89 and 55.93 nm with ease. This would require effective resolutions of several thousand.

- A new concept of Resolving Power is used to differentiate between peak resolution in the IDT and acceptable separation between similar mobility sizes (Resolving power). It is shown that the IDT has a theoretically high Resolving Power for both intermittent push flow and nearly-stopping potential separation.

5.0.2 Future Work

Optimum Design of IDT

The current IDT was a version of old Kanomax DTIMS. It had been used to prove the validity of the concept which has already been achieved. The future work is to model a new IDT instrument for optimum performance. In case of design, the size of the ring electrode (diameter and thickness), the size of spacers(diameter and thickness), the inlet and outlet flow should be checked and calculated. All the design must be validated through the SIMION simulation (using SDS collision model).

A Better Understanding the Flow Behavior

The biggest problem of the current IDT was the flow behavior. As it had two inlets and two outlets, so, it was tough to predict the actual behavior of the flow inside the tube. One important observation was, increasing the annular flow at the inlet the peak became much thinner. More research-works are needed for the flow understanding. In case of the new design of IDT, CFD calculation is a must for predicting the inside flow more accurately, as the movement of charged particles is highly sensitive to flow. At the same time, more research-works are needed to find the advantages and disadvantages of parabolic flow profile as well as flat profile inside the IDT.

Improve the Signal Conditioning

At present, the DAQ being used cannot reach a higher sample rate for the analog input signal. The default sample rate is 1000 cycle/s. A better DAQ with high sample rate will definitely be able to bring out any small hidden signal.

Couple the IDT Prototype with DMA

One important future work is to couple the current IDT instrument with DMA and to check the auto-correction feature. Form the current performance of IDT it is expected to show much better resolution comparing to DMA. A proper validation is needed for that.

REFERENCES

REFERENCES

[1] Gary Alan Eiceman, Zeev Karpas, and Herbert H Hill Jr. *Ion mobility spectrometry.*, CRC press, pages 1-428, 2013.

[2] Herbert H Hill Jr, William F Siems, and Robert H St. Louis. Ion mobility spectrometry. *Analytical Chemistry*, 62(23):1201A–1209A, 1990.

[3] Gary A Eiceman and Craig S Leasure. Ion mobility spectrometer, US Patent 4,7 -77,363., October 11 1988.

[4] Johann Goebel, Christoph Wagner, Ulrich Breit, and Harald Ertl. Ion mobility spectrometer, US Patent 6,479,815., November 12 2002.

[5] Kishore N Vora, John P Carrico Sr, Glenn E Spangler, Donald N Campbell, and Charles E Martin. Ion mobility spectrometer, US Patent 4,712,008., December 8 1987.

[6] Roberto Fernández-Maestre. Ion mobility spectrometry: history, characteristics and applications. *Revista UDCA Actualidad & Divulgación Científica*, 15(2):467–479, 2012.

[7] Richard C Flagan. History of electrical aerosol measurements. *Aerosol Science and Technology*, 28(4):301–380, 1998.

[8] Charlotte Uetrecht, Ioana M Barbu, Glen K Shoemaker, Esther Van Duijn, and Albert JR Heck. Interrogating viral capsid assembly with ion mobility–mass spectrometry. *Nature chemistry*, 3(2):126–132, 2011.

[9] Ching Wu, William F Siems, G Reid Asbury, and Herbert H Hill. Electrospray ionization high-resolution ion mobility spectrometry- mass spectrometry. *Analytical chemistry*, 70(23):4929–4938, 1998.

[10] Alexandre A Shvartsburg and Richard D Smith. Fundamentals of traveling wave ion mobility spectrometry. *Analytical chemistry*, 80(24):9689–9699, 2008.

[11] Tom W Knapman, Joshua T Berryman, Iain Campuzano, Sarah A Harris, and Alison E Ashcroft. Considerations in experimental and theoretical collision cross-section measurements of small molecules using travelling wave ion mobility spectrometry-mass spectrometry. *International Journal of Mass Spectrometry*, 298(1):17–23, 2010.

[12] Roger Guevremont. High-field asymmetric waveform ion mobility spectrometry: a new tool for mass spectrometry. *Journal of Chromatography A*, 1058(1):3–19, 2004.

[13] FA Fernandez-Lima, DA Kaplan, and MA Park. Note: Integration of trapped ion mobility spectrometry with mass spectrometry. *Review of Scientific Instruments*, 82(12):126106, 2011.

[14] J Fernandez de la Mora, Luis de Juan, Thilo Eichler, and Joan Rosell. Differential mobility analysis of molecular ions and nanometer particles. *TrAC Trends in Analytical Chemistry*, 17(6):328–339, 1998.

[15] Laura M Matz, Pete S Tornatore, and Herbert H Hill. Evaluation of suspected interferents for tnt detection by ion mobility spectrometry. *Talanta*, 54(1):171–179, 2001.

[16] Robert Gordon Ewing, David Alan Atkinson, GA Eiceman, and GJ Ewing. A critical review of ion mobility spectrometry for the detection of explosives and explosive related compounds. *Talanta*, 54(3):515–529, 2001.

[17] Souji Rokushika, Hiroyuki Hatano, Michael A Baim, and Herbert H Hill. Resolution measurement for ion mobility spectrometry. *Analytical Chemistry*, 57(9):1902–1907, 1985.

[18] Doug Wittmer, Yong Hong Chen, Brian K Luckenbill, and Herbert H Hill Jr. Electrospray ionization ion mobility spectrometry. *Analytical Chemistry*, 66(14):2348–2355, 1994.

[19] Vasily G Suvorov and Nikolay M Zubarev. Formation of the taylor cone on the surface of liquid metal in the presence of an electric field. *Journal of Physics D: Applied Physics*, 37(2):289, 2003.

[20] Shibdas Banerjee and Shyamalava Mazumdar. Electrospray ionization mass spectrometry: a technique to access the information beyond the molecular weight of the analyte. *International journal of analytical chemistry*, 2012:40, 2012.

[21] E. Cunningham. On the velocity of steady fall of spherical particles through fluid medium. *Proceedings of the Royal Society of London A: Mathematical, Physical and Engineering Sciences*, 83(563):357–365, 1910.

[22] EO Knutson and KT Whitby. Aerosol classification by electric mobility: apparatus, theory, and applications. *Journal of Aerosol Science*, 6(6):443–451, 1975.

[23] Peter H McMurry. The history of condensation nucleus counters. *Aerosol Science & Technology*, 33(4):297–322, 2000.

[24] Shih Chen Wang and Richard C Flagan. Scanning electrical mobility spectrometer. *Aerosol Science and Technology*, 13(2):230–240, 1990.

[25] Mark R Stolzenburg and Peter H McMurry. Equations governing single and tandem dma configurations and a new lognormal approximation to the transfer function. *Aerosol Science and Technology*, 42(6):421–432, 2008.

[26] Charles Hagwood. The dma transfer function with brownian motion a trajectory/monte-carlo approach. *Aerosol Science & Technology*, 30(1):40–61, 1999.

[27] Eric J Davis, Michael D Williams, William F Siems, and Herbert H Hill Jr. Voltage sweep ion mobility spectrometry. *Analytical chemistry*, 83(4):1260–1267, 2011.

[28] Minal Nahin, Derek Oberreit, Nobuhiko Fukushima, and Carlos Larriba-Andaluz. Modeling of an inverted drift tube for improved mobility analysis of aerosol particles. *Scientific Reports*, 7(1): 6456, 2017.

[29] Edward A Mason and Earl Wadsworth McDaniel. *Transport properties of ions in gases,* Wiley Online Library, volume 6, pages 1-486, 1988.

[30] Kang-Ho Ahn, Sang-soo Kim, and Hae-Young Jeong. Condensation particle counter, US Patent 6,980,284., December 27 2005.

[31] HE Revercomb and Edward A Mason. Theory of plasma chromatography/gaseous electrophoresis. review. *Analytical Chemistry*, 47(7):970–983, 1975.

[32] Diana Rosa Hernandez, John Daniel DeBord, Mark E Ridgeway, Desmond A Kaplan, Melvin A Park, and Francisco Fernandez-Lima. Ion dynamics in a trapped ion mobility spectrometer. *Analyst*, 139(8):1913–1921, 2014.

[33] Raymond E March and John FJ Todd. *Practical Aspects of Trapped Ion Mass Spectrometry, Volume V: Applications of Ion Trapping Devices*. CRC press, pages 1-534, 2016.

[34] Hanh Lai, Timothy R McJunkin, Carla J Miller, Jill R Scott, and José R Almirall. The predictive power of simion/sds simulation software for modeling ion mobility spectrometry instruments. *International Journal of Mass Spectrometry*, 276(1):1–8, 2008.

[35] Anthony D Appelhans and David A Dahl. Simion ion optics simulations at atmospheric pressure. *International Journal of Mass Spectrometry*, 244(1):1–14, 2005.

[36] David A Dahl. Simion 3d version 6.0 users manual. Technical report, EG and G Idaho, Inc., Idaho Falls, ID (United States), 95/0403-Rev.4, 1995.

[37] Satendra Prasad, Keqi Tang, David Manura, Dimitris Papanastasiou, and Richard D Smith. Simulation of ion motion in faims through combined use of simion and modified sds. *Analytical chemistry*, 81(21):8749–8757, 2009.